LBL-14504
c.2

Lawrence Berkeley Laboratory
UNIVERSITY OF CALIFORNIA

Materials & Molecular Research Division

RECEIVED
LAWRENCE
BERKELEY LABORATORY

JUN 8 1983

LIBRARY AND
DOCUMENTS SECTION

Presented at the Symposium on Advances in Catalytic Chemistry II, Salt Lake City, UT, June 16, 1982; and to be published in the Proceedings

LOW ENERGY ELECTRON DIFFRACTION (LEED) AND HIGH RESOLUTION ELECTRON LOSS SPECTROSCOPY (HREELS) STUDIES OF MOLECULAR ADSORBATES ON MODEL CATALYST SURFACES

B.E. Koel, M.A. Van Hove, and G.A. Somorjai

December 1982

TWO-WEEK LOAN COPY

This is a Library Circulating Copy which may be borrowed for two weeks. For a personal retention copy, call Tech. Info. Division, Ext. 6782.

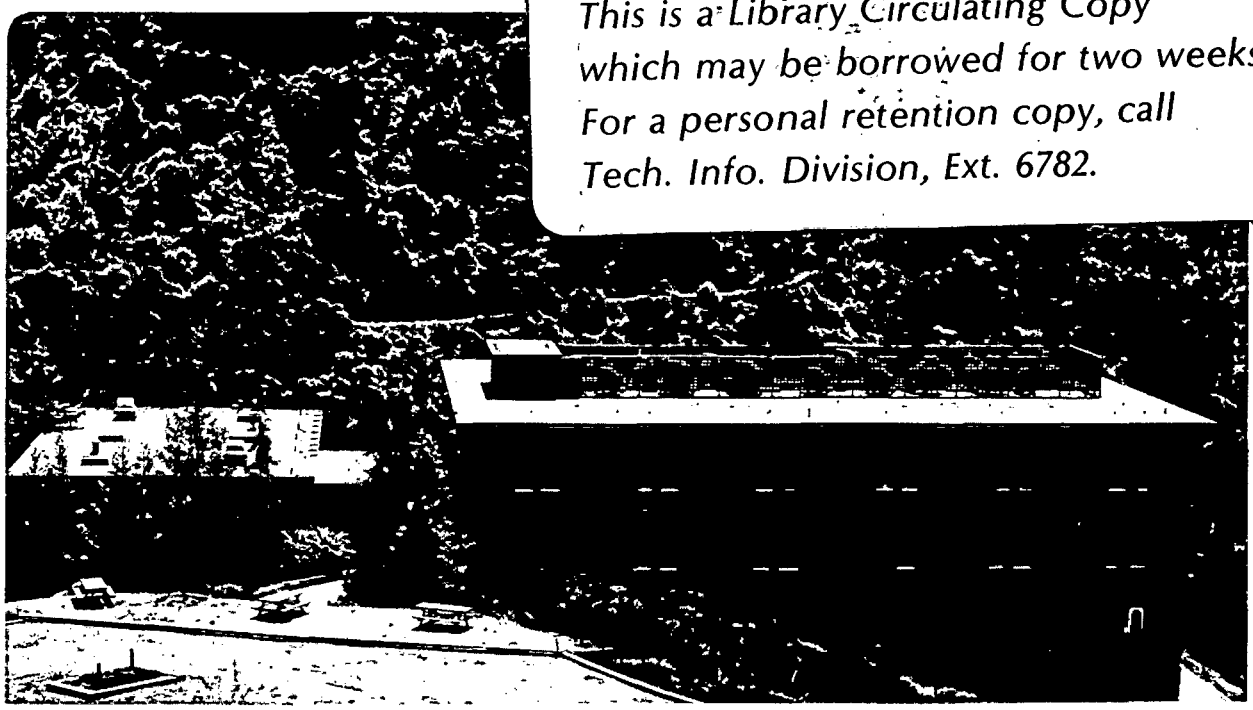

Prepared for the U.S. Department of Energy under Contract DE-AC03-76SF00098

LBL-14504 c.2

DISCLAIMER

This document was prepared as an account of work sponsored by the United States Government. While this document is believed to contain correct information, neither the United States Government nor any agency thereof, nor the Regents of the University of California, nor any of their employees, makes any warranty, express or implied, or assumes any legal responsibility for the accuracy, completeness, or usefulness of any information, apparatus, product, or process disclosed, or represents that its use would not infringe privately owned rights. Reference herein to any specific commercial product, process, or service by its trade name, trademark, manufacturer, or otherwise, does not necessarily constitute or imply its endorsement, recommendation, or favoring by the United States Government or any agency thereof, or the Regents of the University of California. The views and opinions of authors expressed herein do not necessarily state or reflect those of the United States Government or any agency thereof or the Regents of the University of California.

LOW ENERGY ELECTRON DIFFRACTION (LEED) AND HIGH RESOLUTION ELECTRON LOSS SPECTROSCOPY (HREELS) STUDIES OF MOLECULAR ADSORBATES ON MODEL CATALYST SURFACES

B. E. Koel, M. A. Van Hove, and G. A. Somorjai

Materials and Molecular Research Division
Lawrence Berkeley Laboratory
and Department of Chemistry
University of California, Berkeley
Berkeley, California 94720

Abstract

The scattering of low energy electrons is an ideal probe of the structure of surfaces because of the high cross section for both elastic and inelastic electron scattering. The elastically scattered fraction is utilized in low energy electron diffraction (LEED) to determine the structure of clean solid surfaces and of monolayers of adsorbates, atomic or molecular. The discrete loss of electron energy in the excitation of the vibrational modes of atoms and molecules can also be used to determine the surface structure of atoms and molecules. This technique is known as high resolution electron energy loss spectroscopy (HREELS). We shall focus our discussion on the structures of adsorbed CO, several olefins, and several other small molecules that were recently studied by both LEED and HREELS studies.

When adsorbed on metal crystal surfaces, several binding states of CO have been observed that fill as a function of coverage. Acetylene, ethylene, propylene, methylacetylene, and butenes all undergo structural transitions as a function of temperature and are accompanied by drastic changes in bonding. On Pt and Rh single crystal surfaces, the most stable molecular arrangement

for these adsorbed hydrocarbons near room temperature appears to be the alkylidyne structure with the C-C bond axis perpendicular to the metal surface and the molecule anchored to a 3-fold surface site on a (111) plane. Increased temperatures lead to sequential bond breaking and fragmentation. The CH and C_2H fragments appear to be the active species present on transition metal surfaces during catalytic reactions. The vibrational spectra obtained on single crystal and dispersed rhodium particle surfaces will also be compared.

I. INTRODUCTION

In recent years the newly developed techniques of surface science have permitted the study of monolayers of adsorbates on the molecular scale. Since the catalytic action over most heterogeneous catalysts occurs in this monolayer there is intense interest in applying surface science to the scrutiny and better understanding of the elementary steps of catalysis: adsorption, surface migration, molecular rearrangements and bond breaking on the surface, and desorption.

Studies of the structure of adsorbed molecules in the surface monolayer along with the variation of their structures with temperature, coverage, and changes of the substrate structure could reveal the structural possibilities that are permitted for the adsorbates and reaction intermediates that are present on the surface during the catalytic action. If we could combine the study of the adsorbate surface structure with investigation of the catalytic reaction rate parameters (turnover rates, activation energies, selectivities, and structure sensitivity) we could perhaps establish strong correlations between the surface structure of adsorbates and their reactivity. For this purpose we developed the use of single crystals of transition metals as model catalysts. On these surfaces the substrate and adsorbate geometry and configuration could be varied in a controlled manner. The surface structures and composition could be determined under ultra high vacuum (UHV) conditions. Then high pressure reaction studies could be performed using these well-defined crystal surfaces as catalysts in the same apparatus specially developed for this purpose.

In this paper we shall describe two major surface science techniques used in UHV and their impact on the understanding of the structural aspects of molecules adsorbed on metal surfaces. These techniques are High Resolution

Electron Energy Loss Spectroscopy (HREELS) and Low-Energy Electron Diffraction (LEED), both of which use low energy electrons as probes. The use of low kinetic energy electrons gives a high surface sensitivity, because such electrons penetrate the surface by only a few atomic layers before they undergo inelastic scattering. A number of other techniques are available for examining surface structures (such as Infrared Spectroscopy (IR), Ultraviolet (UPS) and X-Ray Photoemission Spectroscopies (XPS), Low-, Medium-, and High-Energy Ion Scattering Spectroscopies (ISS), Surface Extended X-Ray Absorption Fine Structure Spectroscopy (SEXAFS), and others), but we have chosen to rely mainly on HREELS and LEED in our laboratory. The main reasons for this choice are as follows.

HREELS is particularly suited for a quick qualitative determination of the molecular species present at the surface and their mode of bonding to the substrate (bond orders and general conformation). The vibrational frequencies of the surface species measured by HREELS can be compared with IR frequencies of gas-phase molecules and organometallic clusters to aid in the assignment of the adsorbed species. It does not require ordering of the surface species and importantly it can detect hydrogen in the adsorbate through its vibrations with the other atoms in the complex. It can also handle the complications of coadsorption of several different species, especially when the surface species are quite different from each other.

LEED serves well in a complementary fashion to HREELS by enabling bond lengths and bond angles to be determined. Being a diffraction technique, it requires a relatively high degree of ordering of the adsorbates on the surface. Despite the complications due to multiple scattering of the diffracting electrons, LEED has been able to deduce many surface structures to an accuracy

of often better than 0.1 Å. Unlike some of the competing techniques, it has few restrictions on the chemical elements that can be studied (but hydrogen is mostly undetectable). In addition, LEED has been developed over the years into a proven and reliable technique.

Some basic principles and methods of both HREELS and LEED will be described in more detail in the following two Sections. Next, we shall give examples of their use that will illustrate phenomena of direct relevance to heterogeneous catalysis. The chemisorption of CO is chosen for study because of its involvement in important catalytic reactions and as a prototype of more complex systems, clearly exhibiting various modes of molecular bonding to surfaces and bond strength variations due to the nature of the substrate. The important area of hydrocarbon reactions is dealt with and elementary chemical transformations are illustrated with acetylene and ethylene adsorption and decomposition on transition metal surfaces. The adsorption and decomposition of CH_3OH and surface interactions between adsorbed species in the coadsorption of NO and NH_3 or Pt(111) are described. Finally, the case of CO adsorption on a supported metal surface will illustrate the applicability of surface science methods to model catalysts other than single crystals.

II. HIGH RESOLUTION ELECTRON ENERGY LOSS SPECTROSCOPY (HREELS)

HREELS has undergone an explosive development in the last five years due to its ability to extract important structural information about molecular (and atomic) species adsorbed at surfaces.[1,2] Although the instrumentation can be delicate, its use is relatively quick, efficient and versatile, compared to other techniques giving structural information. HREELS has been applied to a number of adsorption systems of great variety.[3] Its potential uses are still partly unknown, as the basic inelastic scattering mechanisms that provide the coupling to surface vibrational modes are continuing to be explored at the present time.

Electrons that are inelastically scattered in the specular direction have undergone a long-range interaction with surface vibrational modes that is similar to the interaction experienced by photons in infrared spectroscopy at surfaces.[4,5] This interaction is called (dynamic) dipole scattering and involves only those vibration modes that have a long wavelength in the direction parallel to the surface (these are small-wavevector modes that therefore can only impart momentum to cause only a small deviation of the electrons away from specular reflection). Note that the large-angle scattering (from the incidence direction to the specular direction) implicit in specular reflection is due mainly to a LEED-like diffraction by the surface, which causes no detectable loss of kinetic energy. A specular HREELS spectrum thus exhibits loss peaks at those energies that correspond to the vibrational frequencies of the molecular (or atomic) species in their adsorbed state on the surface. This allows the ready identification of the adsorbed species by comparison with known frequencies in other circumstances, as in gas-phase molecules and in particular organometallic clusters. Phonons in the substrate can also be detected in this manner;[6] their frequencies generally fall below those of interest in adsorbed molecules.

In dipole scattering from adsorbates on metal substrates an approximate selection rule holds, equivalent to that applicable in IR from metal surfaces, which states that only vibrational modes with a dynamic dipole component perpendicular to the surface can be excited. This selection rule is approximate in two ways. First, it assumes 100 percent reflection of the electrons (or photons in IR) by the substrate. Second, it turns out that actually there cannot exist vibrational modes that have a dynamic dipole purely parallel to the surface, because any vibration parallel to the surface induces an electronic motion with a component perpendicular to the surface, however weak

this may be, in the adsorbate-substrate bonds. Both violations of the selection rule are generally weak and can in many cases be ignored. As a result it is often possible to determine the approximate orientation of a molecular species at a surface by invoking this selection rule, a most powerful feature.

Reflection away from the specular direction is mainly achieved by so-called impact scattering, which is a short-range interaction with short-wavelength surface vibrations; in the limit it becomes the inelastic scattering of an electron by just one atom of the surface. Off-specular HREELS data is at present mainly used because no clear selection rule applies to it. It follows that in this configuration all vibration modes should be detectable, which is a very useful complement to the specularly measured data.

The physical basis of impact scattering is still being investigated, while the transition between impact scattering and dipole scattering is essentially unexplored. New effects may thus still be discovered that can open up unexpected ways of getting information about adsorbed species.

In HREELS a collimated beam of electrons impinge on a surface with a given kinetic energy before impact of 2 to 10 eV with an energy spread of 40 to 100 cm^{-1} (5 to 12 meV; 1 meV = 8.065 cm^{-1}). This monochromatization is achieved by using an electrostatic deflection spectrometer, typically using 127° cylindrical or hemispherical sectors. The scattered electrons are energy-analyzed to a similar resolution by an analyzer that is essentially identical to the monochromator. A spectrometer similar to that of Froitzheim, et al.[7] that we have used for HREELS is shown in Fig. 1. Thermal electrons from a hot tungsten filament are focussed with an Einsel lens onto the monochromator entrance slit. After exiting the monochromator, the monoenergetic electron

beam is focussed on the sample by additional lenses. The sample beam current is 10^{-9}-10^{-10}A. The reflected electrons are focussed on the analyzer entrance slit and energy analyzed to produce a loss (vibrational) spectrum. A channeltron electron multiplier with pulse-counting electronics is used to detect the scattered electrons. For specular reflection, typical elastically scattered intensities are 10^4-10^6 counts per second, while inelastic channels have 1-10^4 counts per second.

Energy losses of the scattered electrons can be measured in the range 200 to 4000 cm^{-1} (25 to 500 meV). Different loss mechanisms can account for scattering intensities when one measures the energy losses of electrons that have been specularly reflected or that have been reflected at other angles ("off-specular"). To study these additional angular effects, many spectrometers (eg. see Fig. 1) have rotatable analyzers. However, even spectrometers built with a fixed geometry can study these effects simply by rotating the sample on axis, since the incident angle is not critical.

At present, HREELS is quite versatile as a structural probe. Its sensitivity allows detection of vibrations with small dynamic dipole moments which, for example, makes adsorbed hydrocarbons relatively easier to study than with IR. Also, a large range of loss energies can be studied, for example, extending below metal-carbon stretching frequencies which are difficult to observe in IR. For strong scatterers, HREELS is sensitive to concentrations of less than 0.1 percent of a monolayer and is ideally suited for studies of single crystal metal surfaces. Thus, studies can be carried out on clean, well-characterized surfaces. HREELS can be easily accommodated in a single vacuum chamber with a variety of surface sensitive probes (LEED, XPS, UPS, Auger Electron Spectroscopy (AES), Thermal Desorption Spectroscopy (TDS)) to

obtain a more complete picture of the structure, bonding, and reactivity of adsorbed monolayers. HREELS is not limited, however, to studies of single crystal surfaces; both disordered and optically rough surfaces can be readily studied. Thus, surfaces similar to those used industrially in catalysis can be investigated. Unlike LEED, it does not require long-range ordering of the surface, thereby giving access to the very important low coverage limit of adsorption where adsorbate-adsorbate interactions are negligible. As a vibrational technique, HREELS is strongly sensitive to weakening or strengthening of the chemisorption bond and molecular distortions caused by adsorbate-substrate or adsorbate-adsorbate interactions. This technique has a much better sensitivity than most surface science probes to non-destructively detect hydrogen present in the adsorbate molecule through its vibration with respect to other adsorbate atoms. However, hydrogen adsorbed alone on a metal surface can in some cases be difficult to detect using HREELS. Few techniques can handle the spectral complications of studies of several different coadsorbed species as well as HREELS. Finally, due to the low incident beam energies and beam currents, HREELS is a non-destructive technique which can be used to probe even the structure of weakly adsorbed molecules or molecules especially susceptible to damage during analysis using other techniques.

There are two main disadvantages of HREELS. First, the assignment of vibrational modes to individual loss peaks may not be unique, given especially the relatively poor resolution as compared to IR. The poor resolution limits somewhat the use of isotopic substitution and the analysis of closely spaced vibrational modes. At present, the resolution in HREELS is limited practically to ~40 cm^{-1} and studies have often been done at ~80 - 160 cm^{-1} (full width at half maximum of the elastically scattered peak). Peak assignments can be

made much more accurately, within 5 cm^{-1}. Developments in spectrometer design, along with construction of a quiet, ultra-stable HREELS power supply,[8] have enabled us recently to obtain spectra from Rh(111) with 20 cm^{-1} resolution. Further advances are expected. The second major drawback is that the maximum pressure under which spectra can be obtained is about 5×10^{-5} torr due to electron gas collisions inside the spectrometer. Thus, surfaces during high pressure catalytic reactions and chemisorption at the solid-liquid interface can not be directly studied. Nevertheless, the combination of a high pressure cell inside of a vacuum system which has HREELS is helping to bridge this gap.[9]

III. LOW-ENERGY ELECTRON DIFFRACTION (LEED)

LEED is a relatively well-established technique for surface structure determination, having started to give reliable results about 1960. There are two main modes of utilization of LEED. The most widespread approach is the observation of the LEED "pattern," which indicates the two-dimensional periodicity of the surface.[10,11] The other approach considers the intensities of diffraction which contain information about atomic positions, bond lengths and bond angles at surfaces.[12,13] We shall discuss these approaches in more detail below.

In LEED, electrons of well-defined (but variable) energy and direction of propagation are diffracted by a crystal surface. Usually, only the elastically (vibrational losses not withstanding) diffracted electrons are considered and we shall do so here as well. The electrons are scattered mainly by the individual atom cores of the surface and produce wave interferences that depend strongly on the relative atomic positions of the surface under examination, because of the quantum-mechanical wave nature of electrons.

The de Broglie wavelength of electrons, λ, is given by the formula λ (in Å) = $\sqrt{150/E}$, where E is measured in eV. In the energy range of 10 to 500 eV the wavelength then varies from 3.9 Å to 0.64 Å, smaller or equal to the interatomic distances in most circumstances. Thus, the elastically scattered electrons can diffract to provide information about the periodic surface structure. The LEED experiment is carried out as follows: a monoenergetic beam of electrons (energy resolution approximately 0.2 eV) in the range of 10 to 500 eV is incident on one face of a single crystal. Roughly 1 to 5 percent of the incoming electrons are elastically scattered and this fraction is allowed to impinge on a fluorescent screen. If the crystal surface is well-ordered, a diffraction pattern consisting of bright, well-defined spots will be displayed on the screen. The sharpness and overall intensity of the spots is related to the degree of order on the surface. When the surface is less ordered the diffraction beams broaden and become less intense, while some diffuse brightness appears between the beams. A typical set of diffraction patterns from a well-ordered surface is shown in Fig. 2.

The electron beam source commonly used has a coherence width of about 100 Å. This means that sharp diffraction features are obtained only if the regions of well-ordered atoms ("domains") are of the order of $(100\ \text{Å})^2$ or larger. Diffraction from smaller size domains gives rise to beam broadening and finally to the disappearance of detectable diffraction from a disordered (liquid-like) surface.

One may distinguish between "two-dimensional" LEED and "three-dimensional" LEED. In two-dimensional LEED one observes only the shape of the diffraction pattern (as seen and easily photographed on a fluorescent screen).[10,11] The

bright spots appearing in this pattern correspond to the points of the two-dimensional reciprocal lattice belonging to the repetitive crystalline surface structure, i.e., they are a (reciprocal) map of the surface periodicities. Therefore, they give information about the size and orientation of the surface unit cell: this is important information, since the presence of, for example, reconstruction-induced and overlayer-induced superlattices is made immediately visible. This information also includes the presence or absence of regular steps in the surface.[14] The background in the diffraction pattern contains information about the nature of any disorder present on the surface.[15] As in the analogous case of X-ray crystallography, the two-dimensional LEED pattern in itself does not allow one to predict the internal geometry of the unit cell (although good guesses can sometimes be obtained); that requires an analysis of the intensities of diffraction. Nevertheless, two-dimensional LEED already can give a very good idea of essential features of the surface geometry, in addition to those mentioned before. Thus, one may follow the variation of the diffraction pattern as a function of exposure to foreign atoms: it is often possible to obtain semi-quantitative values for the coverage, for the attractive and/or repulsive interactions between adsorbates,[16] for some details of island formation,[15] etc. The variation of the diffraction pattern with changing surface temperature also provides information about these interactions (in particular at an order/disorder transition,)[15] while the variation with electron energy is sensitive to quantities such as surface roughness perpendicular to the surface and step heights.[14]

In three-dimensional LEED, the two-dimensional pattern is supplemented by the intensities of the diffraction spots (thereby focusing the attention on the

periodic part of the surface structure, i.e., the ordered regions) to investigate the three-dimensional internal structure of the unit cell. This is most readily done by considering the variation of the spot intensities as a function of electron energy and/or direction of incidence.

Measurements of the diffracted electron beam intensities can be carried out by various techniques that include photographing the fluorescent screen or collecting the electrons at any given angle of emission. The resultant intensity vs. electron energy curves (usually called I-V curves) or I-θ or I-ϕ curves (for variation of the polar and azimuthal incidence angles, respectively), serve as the basis for surface structural analysis. A set of I-V curves from a Pt(111) crystal face is displayed in Fig. 3. They exhibit pronounced peaks and valleys which are indicative of constructive and destructive interference of the electron beam scattered from atomic planes parallel to the surface as the electron wavelength is varied. Often, Bragg peaks (due to simple interference between electrons backscattered from different atomic planes, as in X-ray diffraction) can be identified. However, in addition to these and also overlapping with these, there are usually extra peaks that are due to multiple scattering of electrons through the surface lattice.

The presence of well-defined peaks and valleys in I-V curves indicates that LEED is indeed not a purely two-dimensional surface diffraction technique. There is a finite penetration and diffraction takes place in the first 3 to 5 atomic layers. The depth of penetration affects peak widths markedly: the shallower the penetration, the broader is the diffraction peak. By simulating such I-V curves numerically with the help of a suitable theory,[12,13] it is often possible to determine the relative positions of surface atoms (including

therefore bond lengths and bond angles) and it may also be possible to indicate roughly the thermal vibration state of surface atoms. However, a chemical identification of the surface atoms is not possible with LEED.

In this mode of surface crystallography, LEED has been the most productive technique used to analyze atomic positions, bond lengths and bond angles at surfaces. The largest number of results concern clean single-crystal surfaces and atomic adsorbates on them. These have established the technique on a sound and reliable footing and have served as the necessary base for the more recent studies of adsorbed molecules. Overall, about 140 detailed structures have been determined with LEED so far, of which about 10 involve molecules adsorbed at metal surfaces.

A kinematic theory for X-ray diffraction is sufficient to extract the structure within the unit cell of three-dimensional crystals, but in the case of LEED, multiple scattering of the electrons occurs, because each electron passing a given atom will most likely be scattered by it. This means that most diffracted electrons have undergone more than one scattering event by atoms of the surface, which seriously complicates the interpretation of the diffracted intensities. As a result, the computational effort required to solve a structural problem is relatively much greater than in the case of X-ray diffraction, which means that at present, relatively simpler structures must be examined at surfaces. However, the theoretical methods are still under development and progress in the forseeable future should allow more complicated surface structures to be analyzed.

A parallel between X-ray diffraction and LEED is the lack of sensitivity to hydrogen. For LEED this can often be seen as an advantage, for example, with hydrocarbon species, since the neglect of hydrogen is a major

simplification both in the calculation and in the structural search, while hydrogen positions can often be guessed from the non-hydrogen atom positions.

We must stress an important difference between LEED and X-ray diffraction: the mean-free path for non-vibrational inelastic scattering of electrons at LEED energies is of the order of a few atomic diameters (5-10 Å) in all materials investigated so far, unlike the penetration of X-rays which is of the order of 1 μm or more for metals. The shallow penetration of LEED electrons into the surface, which is caused by the strong atomic scattering and a large probability of losing kinetic energy during the collision with the surface, is of course responsible for the high surface sensitivity of this technique. And this penetration depth turns out to be ideal for determining the relative positions of topmost atoms with respect to each other and to the underlying substrate atoms, so that meaningful bond lengths and bond angles can be extracted.

A structural determination by LEED is carried out as follows. For a given chemical surface composition involving usually a metal single crystal with a simple clean surface structure, and an adsorbate, one must first obtain a well-ordered arrangement of the surface. This is accomplished with suitable heat treatments. Some molecular species will never order: they may either remain disordered because of inadequate intermolecular forces, or they may dissociate in every attempt to order them. However, it is remarkable how many molecular species can be made to order,[11] thus enabling a LEED analysis to be performed.

Once the surface is well prepared, the electron diffraction experiment can start. Normally one measures the intensities of each diffracted beam as a function of the energy of the incident electrons for a fixed direction of

incidence. This can be done directly with a Faraday cup or from the screen with a spot photometer. In more recent approaches, one analyzes photographs of the screen that are then digitized, or vidicon camera images, or the digital output from a position-sensitive resistive anode, all of which can yield beam intensities. These digital methods have been developed in part to enhance the speed of the measurement and reduce the incident beam current; a major reason for this is electron beam damage of the adsorbed molecular species.

The resulting intensity vs. energy plots are called I-V curves and are simulated by corresponding theoretical curves to accomplish the analysis. The theory of LEED is sufficiently complicated that no effective data reduction or inversion method has been developed to directly extract the atomic positions in adsorbed molecular species. It is therefore necessary to simulate the entire LEED process on the computer for a given trial structure and to compare the predicted I-V curves with the measured ones. On the basis of the level of agreement, or lack thereof, between theory and experiment, a new trial structure can be proposed and the process repeated. In practice it is more economical to perform calculations for a series of *a priori* plausible structures and then to assess the situation before starting with a new series of more refined structures, or completely different structures, depending on the success or failure of the first attempt.

It is obviously most useful in such a trial-and-error approach to have independent information that restricts the number of possible structures. Such information can come from any other source, such as other surface sensitive techniques (AES, UPS, TDS, etc.)[11] or chemical knowledge concerning bond lengths and bond angles. For example, HREELS can provide the identity and rough conformation of the surface species at hand, which is usually difficult

to obtain with LEED alone. This, incidentally, illustrates the general situation that a multitechnique approach is very useful in surface studies.

We shall now describe the capabilities and limitations of LEED, bearing in mind that these constantly change as progress takes place. As was mentioned before, there is a requirement that ordering of the surface has occurred to perform a LEED analysis. Also, hydrogen can only be detected in unusual circumstances. But otherwise, all chemical elements produce detectable diffraction when present in an ordered fashion at a surface. For example, even light elements such as carbon and oxygen are strong enough scatterers to be easily detected when they are deposited on a heavy-element substrate such as platinum.

Some limitations that are due to the cost of computing concern the size of the surface unit cell and the complexity of surface layers. Unit cells larger in area than about 50 $Å^2$ are difficult to handle at present; this corresponds for example to a (3x3) unit cell on Pt(111) [the (3x3) notation defines a unit cell of shape and orientation equal to those of the clean substrate unit cell, but 3 times larger in linear dimensions]. Surface layers containing more than about 6 atoms in the unit cell also cause high computational costs. These limitations are alleviated, but not removed, by the use of symmetry and approximate treatments of the multiple scattering.

Adsorbed molecules that have already been studied by LEED intensity analyses are CO and NO, which in some investigations were found to be dissociated rather than associatively adsorbed, acetylene and ethylene, which we shall describe in some detail in the next Section, and C_3 and C_4 straight-chain hydrocarbons. These adsorption systems already include a number of interesting effects that are important for the understanding of the basic mechanisms of heterogeneous catalysis.

IV. EXAMPLES

In this section we discuss applications of LEED and HREELS to several adsorbates on metal surfaces. These systems were chosen because of their topical interest and because of the contributions that these techniques have made to their understanding. We have focused the work in our laboratory on Pt and Rh surfaces and we will mostly discuss studies on these surfaces.

1. Carbon Monoxide Adsorption

1a. Chemisorption of CO on Metal Surfaces. The adsorption of CO has long served as the basic prototype for molecular adsorption on surfaces. It exhibits several features of general interest, which can be studied in considerable detail. Thus, it has long been known that CO can produce non-dissociated ordered overlayers on metal surfaces, yielding sharp LEED patterns. UPS was applied to CO overlayers on metal surfaces and the conclusions were reached that CO most often bonds through its carbon end to the metal and that the adsorption site can vary with the chemical and geometrical nature of the substrate as well as with the coverage (packing) of the overlayer. However, these general conclusions needed confirmation, while it remained difficult to reach specific structural conclusions about individual adsorption systems.

The basic mechanism of CO bonding to metals is by electron transfer from the CO 5σ orbital to the metal d orbitals and by backbonding from the metal d electrons into the CO $2\pi^*$ antibonding orbital which is the lowest unfilled orbital available. This picture has been used to explain the IR spectra of adsorbed CO and of metal carbonyls. The electron density in the CO $2\pi^*$ antibonding orbital is increased, weakening the C-O bond, and the CO stretching frequency (ν_{C-O}) is decreased below the gas phase CO value of 2143 cm^{-1}. The IR spectra of metal carbonyls of known molecular structure

show that as the coordination number of CO to metal atoms is increased ν_{CO} decreases even further.

Many IR studies have been made on supported and polycrystalline samples and these results will not be reviewed here, although they serve as extremely valuable references for interpretation of HREELS data. A large body of HREELS vibrational data has also been published for CO adsorbed on metal single crystals which have well-defined surfaces and adsorption sites.[3]

An important basic question about CO adsorption is the identity of the bonding site. If we limit ourselves to the more likely high-symmetry adsorption sites, there are available sites of 1-fold, 2-fold, 3-fold and 4-fold coordination to metal atoms on the more commonly used single-crystal surfaces, i.e., the carbon atoms could bind to 1, 2, 3 or 4 equidistant metal atoms. With IR applied to metal carbonyl clusters and later with IR and HREELS applied to surfaces, it has been observed that different coordinations show up as different CO stretching frequencies (ν_{C-O}). Specifically, for 1-fold coordination ("terminal bonding," "linear bonding," "one-fold site," "atop site," or "top site") one finds frequencies that vary in the range 2000–2150 cm^{-1} (250–270 meV); for 2-fold coordination ("edge bridging," "bridge site," or two-fold site") the range is 1850–2000 cm^{-1} (230–250 meV); and for higher coordination ("face bridging," "hollow site," "three-or four-fold site") the frequencies fall below about 1850 cm^{-1} (230 meV).

The frequency variations within each of the above ranges are due to differences in bonding from one metal to another and from one crystallographic face to another, and to intermolecular interactions that vary as a function of coverage. As a result of these variations, the frequency ranges for different sites are not well separated, so that it is sometimes difficult to decide which adsorption site is occupied on the basis of the vibrational spectrum alone.

One can use LEED to determine the adsorption site. In addition, LEED gives access to other structural information, such as the tilt angle of the CO molecules with respect to the surface normal and all the bond lengths, and this has indeed been carried out on several CO adsorption systems.

With the accumulated information on CO adsorption on many metal surfaces, the early general picture has been confirmed and refined. In Table I, we list the results for those CO adsorption systems that have been analyzed by both HREELS and LEED. In these cases the CO molecules are found to stand perpendicularly to the surface in either top sites or bridge sites (hollow sites on surfaces are in fact rarely occupied by CO).

For CO adsorption on Ni(100), (111), and (110) surfaces,[17] it was found that for cases where the binding energies for different adsorption sites were not too different, the metal-carbon stretching frequency (ν_{M-C}) is the highest for CO adsorbed in an atop site, smaller for bridge-bonded sites and even smaller for sites of higher coordination. This trend agrees with that expected from calculations that use a simple force constant model. The ν_{M-C} frequencies observed are also consistent with traditional site assignments based on the ν_{C-O} frequencies.

Bertolini and Tardy[17] have compiled data from many HREELS studies of CO adsorbed on metal single crystals. Quantitatively, one sees that the ν_{M-C} mode correlates with the CO binding energy; a weaker adsorption energy (E_{ads}) corresponds to a lower ν_{M-C} frequency. They also showed for CO adsorbed in an atop site at low coverages a linear relationship exists between ν^2_{M-C} and E_{ads}. This is expected if the M-CO chemisorption potentials have the same shape and the force constant f_{M-CO} is proportional to the bond strength (E_{ads}).

LEED, TDS, and UPS studies on the interaction of CO with the hexagonally closest packed faces of the Group VIII metals show numerous similarities. However, this is not true of the vibrational spectroscopy data. CO almost always forms a $(\sqrt{3} \times \sqrt{3})$ R30° surface structure at intermediate coverages. This LEED pattern changes through a number of intermediate steps, possibly into a hexagonal closest packed overlayer of CO molecules or, more likely, into a periodic antiphase domain structure.[18] This is the case despite varying electronic configurations and different metal-metal distances. The desorption energies derived from TDS measurements vary by only 3 kcal/mole on the surfaces where no CO decomposition is detected.[16] Furthermore, the binding energy difference between the $\widetilde{4\sigma}$ and $\widetilde{5\sigma}$ CO molecular orbitals varies by only ±0.3 eV.[16] The vibrational spectra show tremendous differences, however. Both nickel[19] and palladium[20] form multiply coordinated carbonyl species at low CO exposures and the atop species are only seen at high coverage. The CO chemisorption behavior on Rh(111)[21] and Pt(111)[22,23] is the opposite; here the atop sites populate first and predominate at low CO exposures. Bridge bonded species begin to form at intermediate coverages. Ruthenium[24] and copper[25,26] are totally different; only a single C-O stretching vibration is present at all coverages. The reasons for these differences in the nature of CO bonding to the various transition metal surfaces are currently of great interest.

It is found that coadsorbed atoms can affect the extent of backdonation and thus change the CO stretching frequencies. Specifically, electron donors such as potassium, increase the backdonation while electron-withdrawing atoms, such as oxygen, decrease the backdonation. The effect on the CO frequencies can be quite large, as we shall illustrate in a later section. Dissociation of CO

also can occur on various surfaces, for example, on iron.[27] HREELS can easily detect this situation since the CO stretch frequency disappears completely, while new metal-carbon and metal-oxygen vibration frequencies become visible. The dissociated atoms can, in addition, order themselves, yielding a LEED pattern that permits the determination of their positions. Such analysis confirms the expected dissociation by showing that the atoms adopt positions identical to those of oxygen-only or carbon-only overlayers on the otherwise clean metal.

1b. CO Chemisorption on Rh(111)

The application of HREELS and LEED to a specific system is illustrated in more detail in this section on CO adsorption of Rh(111). The HREELS experiments discussed were carried out in our laboratory in an all stainless steel ultrahigh vacuum (UHV) chamber built in two levels. The upper portion contained the standard single crystal surface analysis equipment (4-grid LEED/Auger optics, glancing incidence electron gun and quadrupole mass spectrometer). After dosing, the samples are lowered into the HREELS spectrometer by an extended-travel precision manipulator. The spectrometer is described in detail above (see Fig. 1). The vacuum chamber is lined with layers of μ metal and silicon-iron shielding to reduce stray magnetic fields. The base pressure in the system is maintained at 1×10^{-10} torr with two sputter ion pumps and a titanium sublimation pump. The LEED studies discussed from our laboratory were carried out in a similar single-level chamber, but without HREELS capability.

The HREELS spectra of CO chemisorbed on Rh(111) at 300 K as a function of exposure are shown in Figure 4. At very low exposures (less than 0.1 L; 1L = 1Langmuir = 10^{-6} torr sec) only one peak at 1990 cm^{-1} is observed in

the C-O stretching (ν_{C-O}) region and no ordered LEED pattern is found. By comparison with the infrared spectra of relevant organorhodium compounds[28,29] and with matrix isolated metal carbonyls,[30] one can assign this loss to ν_{C-O} of a linearly bonded species. This peak shifts to higher frequency as the coverage is increased. Possible causes for this include local field effects,[31,32] vibrational coupling,[32] dipole-dipole interactions[33] or a decrease in the metal-carbon backbonding due to the increased number of adsorbate molecules.[34] Figure 4 clearly shows a shift in the Rh-C stretching vibration (ν_{Rh-C}) for this linearly bonded species from 480 cm^{-1} to lower frequency with increasing CO exposure. This shift is consistent with a weakening of the metal-adsorbate bond. No other vibrations corresponding to Rh-C-O bending modes were observed in the specular direction. Invoking the normal dipole selection rule,[4,5] we conclude that the C-O bond is oriented perpendicularly to the surface.

At larger than 0.4L CO exposures, a small shoulder near 1870 cm^{-1} appears in Fig. 4. Again by comparison with relevant model compounds[28,30] one can assign this peak to ν_{C-O} of a bridge-bonded species. Unlike the loss near 2000 cm^{-1}, this peak grows at essentially constant frequency, never varying more than ±5 cm^{-1}. By a CO exposure of 1.0 L the Rh-C stretch has significantly broadened. The new low frequency shoulder appearing slightly above 400 cm^{-1} corresponds to ν_{Rh-C} of the bridge-bonded species. Again, the bridge bonded species is oriented perpendicularly to the surface since no bending or asymmetric stretching modes are observed in the specular direction.

The vibrational spectra of CO chemisorbed on Rh(111) at 300K with increasing background CO pressure are shown in Fig. 5. The C-O stretching frequency for the atop site shifts higher as a function of coverage and reaches

a limiting value of 2060 to 2070 cm^{-1}. The Rh-C stretch of the atop species simultaneously decreases to 420 cm^{-1}. The 1870 cm^{-1} loss due to the bridge bonded species remains at a constant frequency with increasing coverage.

Transmission and reflection IR studies on evaporated Rh films and on supported Rh cluster carbonyls of known molecular structure have also been studied and analogous stretching frequencies in the 1800-2100 cm^{-1} region were observed. For Rh films, weak absorption peaks near 400-575 cm^{-1} were seen indicative of Rh-C stretching and bending vibrations. However, for supported Rh, substrate absorption below 1000 cm^{-1} masked all Rh-C vibrations. Early IR studies[35] of highly dispersed Rh particles supported on Al_2O_3 showed a doublet at 2095 and 2027 cm^{-1} and concluded that a gem dicarbonyl species of the form $Rh(CO)_2$ was formed in addition to linear and bridge-bonded species. The presence of gem dicarbonyl species cannot be ruled out in our studies due to the limited resolution of HREELS, but it seems unlikely[36] because of the high density of metal atoms on the Rh(111) surface that would lead to extreme crowding of CO molecules in the dicarbonyl configuration. Also, in IR studies of Rh films, no $Rh(CO)_2$ species were observed, presumably again due to steric hindrance.

The chemisorption of CO on Rh(111) is completely reversible. As the background pressure of CO is pumped away (Fig. 5), ν_{C-O} for the more weakly bonded bridged species decreases in intensity and ν_{Rh-C} and ν_{C-O} for the atop site shift back into their original positions. The bridge-bonded species can be selectively removed from the substrate by slowly heating the crystal to approximately 360 K in vacuum.[21] No CO decomposition is detected under any of the conditions employed in these experiments ($p \leq 1 \times 10^{-5}$ torr CO, $T \leq 600$ K), evidenced by no new Rh-C or Rh-O stretching vibrations.

We now turn to LEED crystallographic studies performed in our laboratory on the same CO adsorption system.[37] As a function of CO coverage an interesting sequence of LEED patterns is observed, cf. Fig. 6. The clean Rh(111) surface has a LEED pattern (Fig. 6a) consisting of a hexagonal array of spots with the 3-fold symmetry characteristic of the ideal truncation of the unreconstructed bulk Rh lattice. With increasing CO coverage a set of extra spots becomes visible that sharpen up and reach maximum intensity at 1/3 monolayer coverage (Fig. 6b): the corresponding pattern, which again is hexagonal with 3-fold symmetry, is labelled $(\sqrt{3} \times \sqrt{3})R30^\circ$, because the unit cell of the absorbate layer is enlarged by a linear factor $\sqrt{3}$ and rotated 30° with respect to the clean Rh(111) unit cell. At these coverages only one adsorption site is detected by HREELS, namely the top site, cf. Fig. 4.

At higher coverages, the extra spots split up in a complicated fashion, weaken and later reappear as shown in Fig. 6c. By this time, it is difficult to increase the coverage and the CO layer appears to have reached saturation density. (At the temperature of the experiment, ~240K, no CO multilayer growth is possible.) However, by increasing the CO pressure in the vacuum chamber by several orders of magnitude, it is possible to squeeze in a little bit more CO and the end result is the (2x2) pattern seen in Fig. 6d. The CO coverage at this stage is estimated to be 3/4 of a monolayer, corresponding to three molecules per (2x2) unit cell. At coverages just above the one corresponding to the $(\sqrt{3} \times \sqrt{3})R30^\circ$ pattern, HREELS shows loss peaks growing in at bridge-site frequencies and these continue to grow until the (2x2) pattern is achieved.

Both ordered CO structures, $(\sqrt{3} \times \sqrt{3})R30^\circ$ and (2x2), were good candidates for a full LEED analysis, which would permit confirmation of the

site assignment based on vibration frequencies. Our LEED analysis for the 1/3 monolayer structure will be described now in some detail as an illustration of the general procedure of LEED structure determination. Then the 3/4 monolayer structure determination will be discussed more briefly.

Structure determination of Rh(111) + $(\sqrt{3} \times \sqrt{3})R30^\circ$ CO

The experience gained in the LEED analysis of Ni(100)+c(2x2)CO by Andersson and Pendry[38] and by other authors led us to take special precautions in this work. Three difficulties were encountered in the CO/Ni analysis. First, the ordering of CO on Ni(100) is very sensitive to surface perfection and cleanliness. Second, there was a considerable decrease of intensity in the extra diffraction spots during the time needed to collect the I-V curves with a telephotometer. Third, the c(2x2) pattern nucleates quickly as island formation takes place: the extra diffraction spots would reach near maximum intensity far before the optimal coverage of $\theta = 1/2$. In light of this Ni(100)+c(2x2) CO work, we paid particular attention to the surface cleanliness of the Rh(111) crystal, the LEED beam induced damage of the CO overlayer, and the optimal CO exposure values for the $(\sqrt{3} \times \sqrt{3})R30^\circ$ structure.

In our theoretical analysis of the measured I-V curves, we apply a LEED formalism that includes multiple scattering. The rhodium atoms are represented by a bulk band structure muffin-tin potential, which has been used successfully in other LEED work on clean Rh(111) to describe the manner in which electrons are scattered by the atoms. For the C and O atoms, $X\alpha$ muffin-tin scattering potentials calculated for a NiCO cluster have been chosen as these produced good LEED results on a nickel substrate.[39]

Theory and experiment are compared through a set of R-factors (reliability factors) and their average so as to quantify the comparison. If $I_e(E)$ and

$I_t(E)$ are experimental and theoretical I-V curves, respectively, these R-factors are[40]

ROS = fraction of energy range with slopes of opposite signs in the experimental and theoretical I-V curves;

$$R1 = 0.75 \int (I_e - cI_t)dE / \int I_e \, dE;$$

$$R2 = 0.5 \int (I_e - cI_t)^2 dE / \int I_e^2 dE;$$

$$RRZJ = 0.5 \int [(I_e'' - cI_t'') \quad (I_e' - cI_t')/ (I_e' + \max I_e')]dE/(0.027 \int I_e \, dE);$$

$$RPE = 0.5 \int (Y_e - Y_t)^2 / \ (Y_e^2 + Y_t^2) dE,$$
$$Y(E) = L/(1+V_{0i}^2 L^2), \ L = I'/I$$

Here $c = \int I_e \, dE / \int I_t \, dE$; the apostrophe designates differentiation with respect to the energy. RRZJ is the reduced Zanazzi-Jona R factor,[41] while RPE is Pendry's R-factor,[42] both renormalized with a factor 0.5 to match the scale of the other R-factors; V_{0i} is the half-width at half-height of peaks in the I-V curves.

While the final R-factor value for a given surface structure is obtained by averaging over all available diffracted beams with weights proportional to each beam's energy range, we also exploit the differences between R-factors for different beams in the structural search. This is because different beams should simultaneously show minima when the correct surface structure is used,

while with incorrect geometries it would be improbable to obtain this coincidence of minima.

In the first stage of the structural analysis, the clean Rh(111) surface was confirmed to have the ideal bulk structure with a Zanazzi-Jona R-factor value (2xRRZJ) of 0.14 and a Pendry R-factor value (2xRPE) of 0.20. For the Rh(111)+($\sqrt{3} \times \sqrt{3}$)R30° CO structural determination, four adsorption sites were analyzed which may be labelled aaABC...(top site), bbABC...(hcp hollow site), ccABC...(fcc hollow site), and ddABC...(bridge site). The CO molecule was kept perpendicular to the surface in all cases. The hollow sites were easily ruled out by comparison of theoretical and experimental normal-incidence I-V curves, while the bridge site was ruled out with off-normal-incidence I-V curves. The $\theta = 0°$ data produce a minimum average R-factor (using ROS, R1, R2, RRZJ, and RPE) near the layer spacings (d_{RhC}, d_{CO}) = (2.01, 1.02) Å, while the θ=10° and θ=20° data produce minima at (1.945, 1.075) Å and (1.945, 1.085) Å, respectively. Averaging with weights proportional to the amount of data at each angle of incidence produces values of d_{RhC} = 1.95 ± 0.1 Å, and d_{CO} = 1.07 ± 0.1 Å, where the conventional uncertainty of LEED analyses is quoted. We visually interpolate the average R-factor values at the minimum to 0.25 at $\theta = 0°$, 0.20 at $\theta = 10°$, and 0.26 at $\theta = 20°$, averaging out at about 0.23. The corresponding Zanazzi-Jona R-factor is about 0.40 for this structure; the Pendry R-factor is about 0.50 which is to be compared with about 0.50 and 0.40 for CO on Ni (100) and Cu(100),[38] respectively. Respresentative I-V curves are shown in Fig. 7.

An additional structural parameter that was tested is the topmost Rh-Rh interlayer spacing, which was found to be indistinguishable from the clean surface case, i.e., essentially bulk-like.

We observe in the R-factor dependence on d_{RhC} and d_{CO} a feature already noted by Andersson and Pendry[38] for CO on Ni(100); an R-factor contour plot around the minimum can have an elongated elliptical shape with a major-to-minor axis ratio of up to ~4:1. This elongation implies an uncertainty in the carbon position, but not in the oxygen position, as can also be seen by the constancy of the optimum Rh-O distances found at our three incidence directions (3.03, 3.02, and 3.02 Å at θ = 0, 10, and 20°, respectively), while the C position varies by 0.07 Å.

The uncertainty in the carbon position may explain the slight discrepancy between our results (d_{RhC} = 1.95 Å, and d_{CO} = 1.07 Å) and known Rh-C and C-O bond lengths in rhodium carbonyls, which range from 1.82 to 1.91 Å, and from 1.09 to 1.17 Å, respectively, according to a tabulation for terminal bonding in 10 different such carbonyl clusters.[43] In those clusters the Rh-O distance ranges from 2.96 to 3.04 Å. Thus, our determination puts the C atom somewhat far from the metal, but not the O atom.

Our result of top site adsorption for Rh(111)+($\sqrt{3} \times \sqrt{3}$)R30°CO serves as a confirmation of the postulated correspondence in HREELS between adsorption site and vibrational frequency range for CO adsorbed on different metal surfaces. Our result extends this confirmation to other than the fcc(100) substrate face, for which it was established with CO on Ni, Cu, and Pd(100). A summary of these results is included in Table I. It is seen that ν_{C-O} for the Rh(111)+($\sqrt{3} \times \sqrt{3}$)R30° structure is closer to the frequency range associated with a bridge-bonded CO molecule than that for CO on Ni or Cu(100). Such confirmations of the expected sites provide an important calibration of the vibrational techniques in the sense that the knowledge of the CO adsorption site at one coverage or on one crystal face can be used to determine, without

the help of further LEED intensity analyses, the adsorption site (but not necessarily the bond lengths and angles) on other substrate faces, at other coverages or in disordered states.

The Structure of Rh(111)+(2x2)3CO

A more recent LEED analysis of the (2x2) structure of CO on Rh(111) at 3/4 monolayer coverage has also confirmed the HREELS prediction that both bridge sites and top sites are occupied in that dense structure.[44] This is a more complicated analysis, because three molecules fit in each unit cell and there are consequently more structural parameters to fit the experiment, a situation that LEED practitioners are only now learning to handle.

Figure 8 illustrates the general surface arrangement in this case. The figure assumes a hexagonal lattice of molecules (due to the dense packing), all oriented perpendicularly to the surface. However, this choice forces the top-site molecules off the top sites by 0.78 Å, which may not be the most favorable bonding geometry. Our LEED intensity analysis indicates that, while the CO molecular axes are indeed essentially perpendicular to the surface (within about 10°) the top-site molecules appear to move closer to the top sites than illustrated (by about 0.25 Å) but not all the way because of steric hindrance. These "near-top" molecules have a Rh-C bond length of 1.94 ± 0.07 Å [compared with 1.95 ± 0.1 Å in the top-only ($\sqrt{3}$ x$\sqrt{3}$)R30° structure] with a Rh-C-O bond angle of 164 ± 10°, while the C-O bond length is 1.15 ± 0.1 Å (compared with 1.07 ± 0.1 Å in the top-only structure). The bridge-site molecules have a larger Rh-C bond length of 2.03 ± 0.1 Å, with again a C-O bond length of 1.15 ± 0.1 Å. These values are in good agreement with corresponding values found in rhodium carbonyl clusters,[43] where top-site and bridge-site molecules have Rh-C bond lengths of 1.82-1.92 Å and 2.00-2.08 Å, respectively, and C-O bond lengths of 1.09-1.17 Å and 1.14-1.17 Å, respectively.

In conclusion, by combining HREELS with LEED analyses we can present a fairly complete picture of CO chemisorption on Rh(111). At very low exposures a single species is present on the surface located in a top site (ν_{Rh-C} = 480 cm^{-1}, ν_{C-O} = 1990 cm^{-1}). As the coverage increases, the bonding to the surface becomes weaker (ν_{Rh-C} decreases, ν_{C-O} increases, and the TDS peak maximum shifts to lower temperatures.[21,45,46] This process continues until after approximately 0.5 L exposure where a $(\sqrt{3} \times \sqrt{3})R30^\circ$ LEED pattern is seen and all of the adsorbed CO molecules are linearly bonded to individual rhodium atoms, with a Rh-C bond length of 1.95 ± 0.1 Å and a C-O bond length of 1.07 ± 0.1 Å. Above this coverage, a second C-O stretching vibration corresponding to a bridge-bonded species is observed (ν_{Rh-C} ≈ 400 cm^{-1}, ν_{C-O} =1870 cm^{-1}). A "split" (2x2) LEED pattern is seen indicating a loosely packed overlayer of adsorbate molecules. This overlayer structure compresses upon further CO exposure. Throughout this intermediate coverage regime there is a mixed layer of atop and bridge bonded CO species, and we see a continuous growth of all HREELS peaks and a shift in the loss above 2000 cm^{-1}. Two peaks are also visible in the TDS spectra with the bridge bonded CO having a 4 kcal/mole lower binding energy to the surface than the species located in the atop site. With a background pressure of ~1×10^{-6} torr CO at 300 K, a (2x2) LEED pattern forms whose unit cell consists of three CO molecules, two atop and one bridged, in reasonable agreement with the 2:1 peak intensity ratio found in the HREELS spectra. LEED indicates that all CO molecules are still oriented about perpendicularly to the surface in this dense (2x2) structure, with Rh-C bond lengths of 1.94 ± 0.1 Å and 2.03 ± 0.1 Å and CO bond lengths of 1.15 ± 0.1 and 1.15 ± 0.1 Å for near-top and bridge-site molecules, respectively.

1c. CO Chemisorption on Pretreated Rh(111)

Sexton and Somorjai[47] showed that surface pretreatment had a marked effect on the rate of hydrocarbon formation from H_2/CO mixtures over polycrystalline rhodium foils: oxidation enhanced the methanation rate while surface carbon inhibited product formation. The effects of hydrogen, oxygen, and carbon coadsorption on the CO on Rh(111) vibrational spectra have been studied in our laboratory[21] and these results are summarized here.

H_2 pre-adsorption or post-adsorption on Rh(111) at 300 K had no significant effect on the CO vibrational spectra. No Rh-H stretching vibrations were observed in the specular direction, even at H_2 exposures up to several thousand Langmuirs at room temperature. Finally, no changes were seen after heating the crystal to 600 K in 1×10^{-5} torr of a 3:1 H_2/CO mixture for 30 minutes.[48]

Preadsorbed oxygen had a significant effect on the CO vibrational spectrum. O_2 chemisorption on Rh(111) is dissociative at 300 K yielding a single metal-oxygen stretching vibration[21] at 520 cm^{-1} and a second order thermal desorption maximum.[45,49] The formation of bridge bonded CO was strongly inhibited in the presence of chemisorbed oxygen and the atop sites of CO saturated by an exposure of only 1 L CO. Preadsorbed oxygen also decreased the saturation CO coverage, evidenced by smaller loss intensity and a smaller CO thermal desorption peak area.[21] The linearly bonded C-O stretch shifted ~50 cm^{-1} to higher frequency indicating a weaker chemisorption bond. Since oxygen is strongly electron withdrawing; a decrease in the intensity and extent of Rh-CO backbonding might account for these effects. Consistent with this explanation is a decrease of at least 30 cm^{-1} in the frequency of the metal-carbon stretching vibration and a lowering of the CO thermal desorption temperature by ~40 K.[50]

The Rh(111) surface can be covered with carbon by decomposing $5x10^{-7}$ torr of either acetylene or ethylene at 1100 K for 10 minutes and subsequent flashing to 1200 K. Pre-adsorbed carbon had a very strong inhibiting effect on CO chemisorption. This is the same effect it had on the methanation rate.[47] In HREELS, the low inelastic scattering intensity indicated relatively small CO coverages, while the broad elastic peak and high background level were indicative of poor ordering. Consistent with this was a high background intensity in the LEED pattern and a decrease in the CO thermal desorption peak area. Simple site-blocking by the carbon overlayer which covered most of the crystal face allowed only a few sites to be open for CO chemisorption. For the CO that did adsorb, the vibrational peaks shifted slightly and the maximum CO thermal desorption temperature dropped about 10 K,[21] indicative of a decrease in the strength of the chemisorption bond.

1d. CO Chemisorption on Pt(111) with Coadsorbed Potassium

We have used HREELS to study the chemisorption of CO on Pt(111) with preadsorbed potassium.[51] The potassium had a strong influence on the adsorption site and binding energy of CO adsorbed on this surface. Some of these results are discussed here.

Potassium and other alkali metals, which are often used as additives in catalytic systems have been shown to change the binding energy of reactive molecules to metal surfaces. These alkali-induced changes should significantly alter the relative surface concentration and dissociation probability of CO under catalytic conditions and possibly affect both the reaction mechanism and product distribution. As a model catalyst, we have used a Pt(111) surface on which we had previously characterized the details of K adsorption.[52]

In Figure 9, the HREELS vibrational spectra at 300 K for saturation coverages of CO on Pt(111)/K are shown as a function of potassium precoverage. The potassium coverage (θ_K) was varied by depositing about a monolayer (defined here as saturation coverage of K ($\theta_{K=1}$) and corresponding to about one-third of the Pt(111) surface atom density), then annealing to a specified temperature to achieve the desired coverage by desorbing potassium.[52] The surface was saturated with CO by exposure to >10L CO and HREELS spectra were taken. On the clean Pt(111) surface, the 1875 cm^{-1} peak, usually attributed to the stretching vibration of bridge-bonded CO is about one half as intense as the 2120 cm^{-1} peak, attributed to CO bonded in an atop site. The relative intensity of the two vibrational losses varies continuously with potassium coverage such that the peak heights are nearly equal at $\theta_K = 0.10$. The bridge site vibrational loss intensity becomes more than twice that of the linear site at $\theta_K = 0.3$. This shift in intensity can be interpreted as a shift in CO occupation from the linear site to the bridge site. This trend continues with increasing potassium coverage, and by $\theta_K = 0.6$ the linear site is unoccupied with only bridge-bonded CO molecules remaining.

In addition to the change in site occupancy, the vibrational frequency of the top-site CO species gradually decreases from 2120 cm^{-1} for the potassium-free surface, to 2000 cm^{-1} as the potassium coverage is increased to $\theta_K = 0.3$. The vibrational frequency of the bridge bonded CO species is seen to shift even more substantially from 1870 cm^{-1} on the clean Pt(111) surface to 1565 cm^{-1} at a coverage of $\theta_K = 0.6$.

The low frequency region of the spectra is partially obscured due to tailing of the elastic peak. It does show, however, a platinum-carbon stretching frequency at 475 cm^{-1} for CO on clean Pt(111), which broadens as both top and bridge sites become occupied, shifting to 435 cm^{-1} by

$\theta_K = 0.1$. No K-Pt, K-C, or K-O vibrations were identified. TDS spectra for surfaces prepared as in Fig. 9 showed two main effects with increasing θ_K:(1) broadening of the CO desorption curve with a peak maximum originally at 400 K moving to 600 K by $\theta_K = 0.4$ML, and (2) a decrease in the saturation coverage of CO. Assuming first order desorption kinetics and a preexponential factor of 1.25×10^{15} sec^{-1} as determined by Campbell et al.,[53] this corresponds to an increase in the heat of desorption from 27 to 39 kcal/mole.

The changes in CO vibrational spectra for various CO coverages with constant $\theta_K = 0.3$ are shown in Fig. 10. The top-site CO species (with $\nu_{C-O} = 2000$ cm^{-1}) completely desorbs by 400 K. The bridge-bonded species ($\nu_{C-O} = 1725$ cm^{-1}) maintains approximately the same vibrational peak intensity after heating to 400 K although some peak braodening and decrease in frequency ($\Delta\nu \sim 40$ cm^{-1}) does occur. This should be contrasted with CO desorption from clean Pt(111), where only bridge-bonded species (1870 cm^{-1}) desorb by 400 K, and all of the top-sites (2121 cm^{-1}) are left filled. The asymmetric broadening of the bridge bonded peaks at 1725, 1685, and 1605 cm^{-1} toward lower frequency, combined with high frequency tailing of the 1550 and 1520 cm^{-1} peaks may indicate the occupation of an additional adsorption site on the Pt(111) surface, possibly a three-fold hollow position. Upon further heating the intensity and the stretching frequencies of the multiply bonded species continue to decrease. Finally, when only a small fraction of a monolayer of CO is left adsorbed, ν_{C-O} is 1400 cm^{-1}. This is lower than any previously reported CO vibrational stretching frequency.

We believe that enhanced electron back-donation from the platinum to the CO due to the presence of potassium, is the dominant factor causing the large changes in the adsorption energy, vibrational frequency, and site selectivity

of adsorbed CO. Back donation into the $2\pi^*$ antibonding orbital of CO weakens the carbon-oxygen bond, lowers the CO stretching frequency, and strengthens the metal-carbon bond, increasing the Pt-C stretching frequency. The response of the surface to potassium is best understood as electron transfer from the potassium atom to the platinum valence bands. This is combined with electrostatic screening of the resultant positive charge by the metal electrons. From these results, this effect appears to be delocalized over a few interatomic distances.

Importantly, HREELS data can rule out direct interactions between the adsorbed potassium and CO as a dominant factor inducing the coadsorption changes, since different HREELS peaks (from interacting and non-interacting CO) were not observed at low potassium coverages.

The catalytic implications of the results shown above, especially the weakened C-O bond, are significant. An increase in the electron back-donation from a metal increases the probability of both the hydrogenation of the weakened CO molecule and the dissociative adsorption of CO. For the Fischer-Tropsch reaction ($CO + H_2 \rightarrow$ hydrocarbons), an increase in the rate of CO dissociation will increase the carbon and oxygen surface coverage relative to that of hydrogen. Work in the past[54,55] on catalytic hydrocarbon reactions have shown a preference for longer chain hydrocarbons as well as oxygenated products when alkali oxides were added to catalysts. More exact reaction studies, combined with atomic-level surface characterizations such as those presented here, will eventually lead to a more fundamental understanding of promoter effects in catalysis.

2. The Structure of Alkynes and Alkenes Bonded to the Rh and Pt(111) Surfaces

The molecular basis of many macroscopic surface phenomena that include adhesion, lubrication, wettability, and heterogeneous catalysis of organic

reactants is the structure and bonding of monolayers of adsorbed hydrocarbons. The strength and orientation of the metal-hydrocarbon bond plays a very important role in determining the reactivity and the stability of adsorbed organic molecules. HREELS and LEED in particular have contributed greatly to the study of the structure of small hydrocarbons (up to C_4) on single-crystal metal surfaces, especially Rh(111) and Pt(111).

Chemisorption of Acetylene and Ethylene

The structure of acetylene and ethylene adsorbed on transition metal surfaces is of fundamental importance in catalysis. An understanding of the interaction of these simple molecules with metal surfaces may provide information on possible surface intermediates in the catalytic hydrogenation/dehydrogenation of ethylene. HREELS is a particularly useful probe for studying the hydrocarbon-metal interaction because of both its sensitivity to hydrogen and its broad spectral range, which includes M-C stretching vibrations, C-C stretching vibrations, and C-H stretching and bending vibrations. Here we demonstrate the power of this technique by reviewing the results of an investigation on the adsorption and decomposition of C_2H_2 and C_2H_4 on Rh(111).[56] LEED also contributes significantly by determining the bonding site, the bond lengths and the bond angles for the non-hydrogen atoms.[57]

HREELS Studies of Acetylene Chemisorption on Rh(111)

The vibrational spectrum of the (2x2) hydrocarbon surface structure formed from the chemisorption of C_2H_2 on Rh(111) between 210 and 270 K is shown in Fig. 11. The peak positions and their relative intensities are listed in Table II. Although some of the peaks are not readily visible in Fig. 11, their positions and intensities are obtained from the analysis of at least six

spectra. A complete analysis of the low frequency region in this spectrum is hampered by a spurious background peak near 800 cm^{-1}, indicated by dashed lines. As a result of this experimental artifact (which is not inherent to HREELS), both the position and intensity of all loss features between 650 and 900 cm^{-1} are rather uncertain. Isotopic substitution helps in assigning the observed vibrational frequencies to normal modes of the adsorbed species. The HREELS spectrum of the (2x2) C_2D_2 surface structure is shown as the middle trace in Fig. 11.

The frequencies of the C-H (C-D) stretching vibrations can be used to characterize the state of hybridization of the adsorbed species. Acetylene, C_2H_2 (C_2D_2) is sp hybridized in the gas phase and has C-H (C-D) stretching vibrations between the 3289 and 3374 (2439 and 2701) cm^{-1} [Ref. 58]; ethylene, C_2H_4 (C_2D_4) is sp^2 hybridized and has C-H (C-D) stretching vibrations between 2989 and 3106 (2200 and 2345) cm^{-1}; while ethane, C_2H_6 (C_2D_6) is sp^3 hybridized and has C-H (C-D) stretching vibrations between 2896 and 2985 (2083 and 2235) cm^{-1}. Thus, the losses at 2980 (2230) and 3085 (~2320) cm^{-1} in Fig. 11 correspond to the C-H (C-D) stretching vibrations of a molecule near sp^2 hybridization. This indicates that the C-C-H (C-C-D) bonds in adsorbed acetylene are no longer linear. The low frequency mode at 323 cm^{-1} does not shift significantly (~20 cm^{-1}) upon deuteration and most likely corresponds to the entire molecule vibrating against the surface. The two largest peaks in the spectrum at 706 and 887 cm^{-1} shift by almost 200 cm^{-1} (to 565 and 686 cm^{-1}, respectively) when C_2D_2 is chemisorbed and can be assigned to C-H (C-D) bending modes. A more detailed discussion of these mode assignments, including reference to the IR spectra of model organometallic compounds, is presented in Ref. 56. We

assume the adsorbate is oriented with its C-C axis approximately parallel to the surface since only small, broad peaks (1300-1400 cm^{-1}) are seen in the C-C stretching region. Observations of such a mode in the specular direction is prohibited by the normal dipole selection rule if the C-C bond is parallel to the surface.

Bond lengths, bond angles and the position of adsorbed C_2H_2 on the surface cannot be accurately determined without a complete dynamical LEED intensity analysis, which has not been performed yet. Nevertheless, the HREELS results indicate that acetylene chemisorbs on Rh(111) below 270 K with its C-C axis oriented approximately parallel to the surface. The molecule is near sp^2 hybridization and therefore the C-C-H bond angle is no longer linear. A similar C_2H_2 geometry is seen in numerous organometallic cluster compounds.[59,60]

Both LEED and HREELS indicate that the (2x2) acetylene overlayer is stable on the surface in vacuum between 210 and 270 K. The addition of H_2 to adsorbed C_2H_2 below ~260 K causes no changes in the observed HREELS spectra, although this surface species is still quite active. The addition of H_2 to chemisorbed C_2D_2 below 260 K results in a complex vibrational spectrum with peaks in both the C-H and C-D stretching and bending regions. Although the deuterium and hydrogen readily exchange, <u>no</u> change in the adsorbate geometry is detected by HREELS. The vibrational spectra of adsorbed acetylene only begin to change when the crystal is heated above 270 K in vacuum. The (2x2)-C_2H_2 surface structure also disorders at this temperature.

The vibrational spectrum from the c(4x2) acetylene overlayer is shown in the lower trace of Fig. 11. This spectrum can either be obtained by warming

the (2x2) acetylene overlayer to ~270 K in the presence of $1x10^{-8}$ torr of hydrogen or by chemisorbing C_2H_2 on Rh(111) above 300 K. Hydrogen addition to the surface species above 270 K is necessary to obtain good quality, intense HREELS spectra. However, hydrogen addition was also required to complete this conversion in the LEED studies. This species is stable on the surface up to ~420 K. The structure of this hydrocarbon overlayer will be discussed in more detail in the next section.

HREELS and LEED Studies of Ethylene Chemisorption on Rh(111)

The vibrational spectra from the (2x2) and c(4x2) ethylene surface structures are shown in the two lower traces of Fig. 12. The HREELS spectrum in the lowest trace of Fig. 12 is obtained by chemisorbing C_2H_4 on the crystal below 270 K. The middle trace can either be observed by slowly warming the (2x2) overlayer structure to room temperature or by simply adsorbing ethylene on the Rh(111) surface above 290 K. Small peaks in the 1800 to 2100 cm^{-1} region are due to background CO adsorption. Once again the observed vibrational frequencies are independent of surface order and hydrocarbon exposure (<0.2 to >50 L). Note that these HREELS spectra are almost identical to the vibrational spectrum from the stable c(4x2) acetylene overlayer shown in Fig. 11. The hydrocarbon species derived from ethylene chemisorption is also stable on the surface up to ~420 K. Degradation of both the c(4x2) LEED pattern and of the vibrational spectrum occur at this temperature.

It is interesting to note that the geometry of the adsorbed ethylene species on Rh(111) appears to remain the same, as indicated by the HREELS spectra, while the overlayer structure changes from (2x2) to a c(4x2). Although this conversion is not affected by the presence of hydrogen, H-D

exchange will occur in the hydrocarbon overlayer when H_2 is added to chemisorbed C_2D_2. No change in the adsorbate geometry is detected by HREELS.

The stable ethylene or acetylene plus hydrogen overlayer on Rh(111) can be decomposed to surface CH (CD) species above ~420 K. The HREELS spectra for these two hydrocarbon fragments are shown in Fig. 15. Assignment of the observed vibrational frequencies is discussed in detail by Demuth and Ibach for the decomposition of acetylene on Ni(111).[61] It is possible that species such as these are important surface intermediates under high pressure catalytic conditions.[62]

The HREELS spectrum resulting from the chemisorption of either C_2H_4 or C_2H_2 plus H_2 on Pt(111) above room temperature are quite similar.[63] This species is similar to the hydrocarbon species ethylidyne ($\equiv C-CH_3$ or C_2H_3) obtained from the adsorption of ethylene on Rh(111). This is clearly shown in Fig. 14. A more complete discussion of the similarities between the chemisorption of ethylene on Rh(111) and Pt(111) is presented elsewhere.[56] This stable hydrocarbon species is identical to the hydrocarbon species formed from the chemisorption of either C_2H_4 or C_2H_2 plus H_2 on Pt(111) above 300 K. Decomposition of these molecules to surface CH (CD) species occurs on Rh(111) above ~420 K.

A LEED analysis was performed of the stable hydrocarbon species identified as ethylidyne, which was obtained from either C_2H_2 or C_2H_4 on both Pt(111) and Rh(111) in a (2x2) lattice. We shall describe here the structural determination for ethylidyne on Rh(111).[57]

Four different adsorption sites were tested for the Rh(111)-(2x2)-C_2H_3 determination; they are the atop (aaABC...), the hcp hollow (bbABC...,

xbABC..., and bACB...), the fcc hollow (ccABC...), and the bridge (ddABC...) sites. (The notation aaABC..., etc. indicates lateral layer positioning as in the ABCABC... stacking arrangement of bulk fcc lattices; lower-case letters refer to carbon atoms, d designating a bridged location and x a general location.) The two hollow sites are distinguished by the presence (hcp) or absence (fcc) of second layer atoms directly beneath them. At each site, the carbon-carbon axis was kept perpendicular to this surface except for the hcp hollow (xbABC...) where the axis was tilted from 28 to 42° from the normal along the [011] direction; the carbon-carbon and carbon-metal distances were then varied in 0.1 Å increments.

The comparison between theoretical and experimental I-V curves (nine independent beams) at normal incidence eliminated the atop (aaABC...) and fcc hollow (ccABC...) sites as well as the models with a tilted carbon-carbon axis (xbABC...) and with a quarter monolayer of atomic carbon (bABC...).

To confidently distinguish between the remaining hcp hollow (bbABC...) and bridge (ddABC...) sites, we moved to the intensity curves (thirty-nine independent beams) taken at the three off-normal incidence angles. These clearly favored the hcp hollow site. The importance of off-normal incidence intensity curves to help distinguish between two closely competing structural models has already been observed in the LEED determination of Pt(111)-(2x2)-C_2H_3.[64]

Our analysis gives the projected metal-carbon ($d_{\perp RhC}$) and carbon-carbon ($d_{\perp CC}$) distances to be 1.31 ± 0.1 Å and 1.45 ± 0.1 Å, respectively; these values represent weighted averages over the polar-angle data that account for the different number of beam profiles at each angle. An ethylidyne species is strongly implied by these bond distances consistent with the HREELS work.

Comparison of Ethylidyne Adsorbed on the Pt(111) and Rh(111) Surfaces

The LEED determination of the Pt(111)-(2x2)-C_2H_3 structure[64] showed that ethylidyne stands above an fcc hollow site, while our study clearly indicates that ethylidyne stands above an hcp hollow site on the Rh(111) surface. A possible explanation why ethylidyne would select slightly different adsorption sites on the Pt and Rh surfaces involves the role of coadsorbed hydrogen. TDS studies of the Rh(111)[56] and Pt(111)-(2x2)-C_2H_3 (Ref. 65) overlayers show that the extra hydrogen released to form ethylidyne from ethylene remains on the Rh surface (<270K) but desorbs from Pt(300K). Since hydrogen has been observed to dissociate and sit above a hollow site on the Ni(111)[66,67] and Pt(111)[68] surfaces, it is possible that the coadsorbed hydrogen on the Rh(111) surface may occupy a fcc hollow site and thereby block this site for ethylidyne adsorption.

In Table III, we list the bond lengths for ethylidyne on Rh(111) and Pt(111). We notice that the carbon-carbon distance is longer and the carbon covalent radius shorter for Pt than Rh. These differences may possibly be explained by the different hollow sites that ethylidyne occupies on Rh and Pt.

The Structures of C_3 and C_4 Alkenes Adsorbed on Pt(111) and Rh(111)

LEED I-V curves obtained by adsorption of propylene, methylacetylene, and the 2-butenes on the Pt(111) face at room temperature indicate the formation of propylidyne and butylidyne species;[69] these species are illustrated in Figs. 15 and 16. Methylacetylene in the presence of background hydrogen ($<10^{-9}$ torr) and also propylene produce nearly identical intensity curves as ethylene or acetylene.[69] Since thermal desorption experiments[65] indicate that the carbon skeleton remains intact upon adsorption, the virtual identity in the intensity curves implies that the methyl group in propylidyne is

randomly oriented and thereby does not change the intensity spectra by its presence. The bond lengths and angles determined for ethylidyne carry over for this propylidyne species.

At low exposures (~10L), cis- or trans-2-butene adsorbed on Pt(111) at room temperature produce I-V spectra that are also very similar to the stable ethylene or acetylene intensity curves; but in this case diffuse spots appear in addition to the (2x2) diffraction spots. At higher exposures, the I-V spectra become less similar to the ethylene or acetylene curves, while the extra diffraction spots form a clear $(2\sqrt{3}x2\sqrt{3})R30^\circ$ pattern. This sequence implies the formation of the butylidyne species at low exposures which has its ethyl group disordered, while at higher exposures, the ethyl groups, due to their mutual Van der Waals repulsion, form a $(2\sqrt{3}x2\sqrt{3})R30^\circ$ superlattice,[69] as illustrated in Fig. 17.

Paralleling the adsorption behavior of Pt(111), propylene adsorbed on the Rh(111) face at 230-250 K yields a $(2\sqrt{3}x2\sqrt{3})R30^\circ$ unit cell. Once again high exposures are necessary to completely order the unit cell, while at low exposures the propylene half-order intensity curves strongly resemble the ethylene curves. The fact that Rh(111) already orders a C_3 hydrocarbon into the $(2\sqrt{3}x2\sqrt{3})R30^\circ$ unit cell, while Pt(111) only orders the C_4 can be explained by the smaller (4 percent) lattice spacing of Rh; this forces neighboring molecules to approach each other more closely. LEED analysis is currently underway in our group to confirm the alkylidyne models for the high exposure $(2\sqrt{3}x2\sqrt{3})R30^\circ$ phase on the Rh(111) and Pt(111) surfaces.

3. Reactions of Other Small Molecules with Metal Surfaces

3a. Methanol Decomposition on Pt(111). The adsorption and decomposition of methanol on metal surfaces has been a subject of interest primarily in

connection with the catalytic synthesis of methanol from CO and H_2. Chemisorption studies in UHV of the decomposition or reaction of methanol have shown that formaldehyde can be formed on oxygen covered Ag or Cu surfaces, by way of a methoxy surface intermediate. On other metals (Pt, Pd, Ni, Ru, W) only CO and H_2 are formed. Hydrogenation of a methoxy (CH_3O–) intermediate is also thought to account for the synthesis of methanol from CO and H_2 at high pressures. The identification of a surface methoxy species on metal surfaces under various conditions, and a determination of its stability, could be an important basis for understanding catalytic selectivity and reactivity. HREELS has been shown to be particularly valuable in studies like these. In particular, one can quite clearly distinguish between CH_3OH(ice), and adsorbed species (denoted (a)) $CH_3OH_{(a)}$, $CH_3O^-_{(a)}$, and $CO_{(a)} + H_{(a)}$. This is especially true when HREELS is combined with TPD.

HREELS of a solid multilayer of molecular CH_3OH on Pt(111)[70] gives losses at 680 cm^{-1} (OH bend), 970 (C-O stretch), 1410 (CH_3def), 2930 (C-H stretch), and 3220 cm^{-1} (OH stretch). An HREELS study on Cu(100)[71] and IR spectra of CH_3OH(ice)[72] give similar results.

Desorbing the multilayers of CH_3OH often leaves, at low temperatures, $CH_3OH_{(a)}$. This weakly chemisorbed molecule is adsorbed via the oxygen lone pair electrons. On Pt(111)[70] the C-H stretching (ν_{C-H}) modes are shifted upward by ~60 cm^{-1} due to decreased intermolecular H-bonding and "soft" ν_{C-H} modes appear below 2930 cm^{-1}, presumably due to interaction of the methyl group with the surface Pt atoms.

On Pt(111),[70] warming a multilayer of CH_3OH to 300 K results in complete decomposition to form coadsorbed H and CO. Characteristic bands due to linear CO are found at 470 cm^{-1} (ν_{Pt-C}) and 2080 cm^{-1} (ν_{C-O}). A

band at 1200 cm^{-1} was ascribed to $H_{(a)}$. However, if a multilayer of CH_3OH condensed on top of a p(2x2) $O_{(a)}$ layer on Pt(111) is warmed to 170 K, a methoxy species is formed. This is indicated by the disappearance of the OH bands at 680 and 3210 cm^{-1} and the appearance of a new ν_{Pt-O} band at 370 cm^{-1}. The frequencies and assignments of the methoxy bands on O/Pt(111) are: 370 cm^{-1} (ν_{Pt-O}), 1000 cm^{-1} (ν_{C-O}), 1430 cm^{-1} (CH_3def), and 2910 cm^{-1} (ν_{C-H}). The methoxy species was observed to decompose on O/Pt(111) above 170 K to form $CO_{(a)}$ + $H_{(a)}$. Further heating resulted in desorption of the coadsorbed species to give a clean surface.

Sexton[70] concluded that high CO and H_2 chemisorption heats resulted in the instability of methanol and methoxy species at temperatures above 300 K on Pt, W, Ru, Ni, and Pd at low pressures. This was contrasted with the behavior of Ag and Cu surfaces which have low heats of adsorption for CO and H_2 and form relatively stable methoxy species which decompose to form gaseous formaldehyde and H_2. Thus, the catalytic selectivity of the latter surfaces can be understood.

3b. <u>The Adsorption and Reaction of NO and NH_3 on Pt(111)</u>

The coadsorption and reaction of NH_3 and NO on Pt(111) has been characterized through the use of HREELS and TDS.[73] A brief overview of these studies is given here to illustrate another powerful use of HREELS as a probe of interactions of coadsorbed surface species.

On Pt(111), NO adsorption is molecular. At low NO coverage the adsorption is primarily into bridge sites (ν_{N-O} = 1490 cm^{-1}). As the coverage of NO is increased, terminally bonded NO (ν_{N-O} = 1710 cm^{-1}) forms from the bridge-bonded species to dominate at high coverages.

Molecular adsorption of NH_3 predominates on Pt(111) below 400 K and two different forms of $NH_{3(a)}$ exist under certain conditions of coverage and

temperature. The dominant vibrational band for the low coverage, high temperature form is at 1090 cm^{-1} (sym. band). Post-adsorption of a complete monolayer of NO on this surface at 100 K shifts both NO vibrational bands down by ~80 cm^{-1} and shifts the NH_3 band up by ~150 cm^{-1}, illustrating the interactions between the coadsorbed species.

A surface complex forms upon heating this adlayer to 300 K, characterized by a single broad band at 1280 cm^{-1}. Details of the surface complex are not yet clear, but this strong interaction is confirmed by TDS. Importantly, no direct N_2 formation from the complex was detected. Understanding this complex should yield new information on N/O/H interactions on Pt surfaces.

4. Application of HREELS to the Study of CO Adsorption on Model Supported Metal Catalysts

Most HREELS experiments to date have employed well characterized single crystal substrates under ultrahigh vacuum conditions. These types of substrates are not exclusive, and Dubois et al.[74] extended previous HREELS experiments on single crystal rhodium surfaces to include studies of the chemisorption of CO on model rhodium on alumina catalysts.

Figure 18 is a cross sectional view of a model supported metal catalyst. This surface[74] was prepared by: (1) Evaporating from 200 to 2000 Å average thickness of Al from an aluminum wire on a stranded tungsten filament onto a clean metal substrate. The metal deposition rate was ~10 Å/sec. The evaporated aluminum layer was polycrystalline with grain sizes on the order of microns;[75] (2) Oxidizing this aluminum in oxygen or air at exposures ranging from 1000 L to greater than 10^6 L at temperatures between 300 and 480 K. Aluminum oxidized in this manner has been shown to resemble γ alumina in both its physical and catalytic properties.[76] The polycrystalline oxide layer

was typically 10 Å thick;[77] the grain size is not known. (3) Evaporating from 1 to 20 Å average thickness of Rh from a rhodium wire wrapped around a stranded tungsten filament in $1x10^{-5}$ torr of CO. The metal deposition rate was ~0.25 Å/sec. Rhodium evaporated in this manner has been shown to agglomerate into small, highly dispersed particles on the alumina support.[75] Kroeker et al.,[75] using the same type of rhodium sources, source to substrate distances, and oxidized aluminum substrates, found with transmission electron microscopy that typical Rh particle diameters were 20-30 Å for a 4 Å average thickness. These particles are similar in both size and distribution to those formed from the reduction of transition metal salts on alumina to prepare commercial catalysts.

The lower trace in Fig. 19 is the HREELS spectrum of the oxidized aluminum substrates. The most prominent feature in this spectrum can be assigned to the aluminum oxide phonons. It is a broad band centered just below 900 cm^{-1} and asymmetric to lower energies. This relatively intense alumina phonon band is similar in both position and shape to the peak found by inelastic electron tunneling spectroscopy.[76b,78] A relatively broad, weak band between 3500 and 3600 cm^{-1} correspnding to the O-H stretching mode of surface hydroxyl groups is generally seen in both the infrared[79] and inelastic electron tunneling spectra[76] of γ alumina.

The middle and upper traces of Fig. 19 show the vibrational spectra of CO chemisorbed on the highly dispersed rhodium particles supported on the alumina. These spectra have a smaller expansion scale than the alumina spectrum (x10 as compared to x30) and this represents a relatively large ratio of inelastic electron scattering to elastic electron stretching. For a 4 Å average thickness of evaporated rhodium (middle trace) the intensity of the aluminum oxide

phonon band is significantly decreased. For a 20 Å average thickness of rhodium (upper trace) this phonon mode has completely disappeared. The low frequency loss at 430 cm^{-1} is typical of Rh-CO stretching and bending modes, while the two losses near 2000 cm^{-1} are characteristic of C-O stretching vibrations.

Figure 19 clearly shows that we are now able to obtain HREELS spectra from CO adsorbed on model rhodium on alumina catalysts. We find that charging does not present a problem because the oxidized aluminum layer is thin enough (10-15 Å) to allow relatively low impedance electron tunneling. Experimentally we find that though both the elastic and inelastic peaks are broader in their angular distribution when compared to scattering from a clean Rh(111) surface, the intensity loss is not severe enough to prevent the measurements. We find that the elastic peak intensity (I_0) is down by roughly an order of magnitude; the inelastic peak intensity (I_s) is down by less than an order of magnitude.

Figure 20 compares the HREELS loss spectra of the current work to previously obtained inelastic electron tunneling[75] and infrared spectra[80] of CO on rhodium supported on alumina. Some of the advantages and disadvantages of the various techniques are clear in this figure. Infrared spectroscopy has the best resolution, but the spectrum is obscured in the low frequency region. Tunneling spectroscopy has reasonably good resolution and intensity in the low frequency region, but questions about the effects of the top metal electrode on the vibrational frequencies are not fully answered in the existing literature. The HREELS results in Figure 20 seem to represent an envelope of the IR results in the CO stretching frequency region.

Acknowledgements:

This work was supported by the Director, Office of Energy Research, Office of Basic Energy Sciences, Materials Sciences Division of the U.S. Department of Energy under contract DE-AC03-76SF00098.

REFERENCES

1. H. Ibach and D. L. Mills, "Electron Energy Loss Spectroscopy and Surface Vibrations," Academic Press, (New York), 1982.
2. B. Sexton, Appl. Phys. A26 1 (1981).
3. P. Thiry, in "Vibrations at Surfaces," R. Caudano, J. M. Giles and A. A. Lucas (Eds.), Plenum Press, (New York), 1982, p. 231.
4. E. Evans and D. L. Mills, Phys. Rev. B5 4126 (1972).
5. H. Ibach, Surf. Sci. 66 56 (1977).
6. S. Lehwald and H. Ibach, in "Vibrations at Surfaces," R. Caudano, J. M. Gilles and A. A. Lucas (Eds.), Plenum Press, (New York), 1982, p. 137.
7. H. Froitzheim, H. Ibach and S. Lehwald, Rev. Sci. Instrum. 46 1325 (1975).
8. J. E. Katz, P. W. Davies, J. E. Crowell and G. A. Somorjai, Rev. Sci. Instrum., 53, 785 (1982).
9. A. L. Cabrera, N. D. Spencer, E. Kozak, P. W. Davies and G. A. Somorjai, J. Vac. Sci. Technol., in press.
10. G. Ertl and J. Küppers, "Low Energy Electrons and Surface Chemistry," Verlag Chemie (Weinheim, Germany), 1974.
11. G. A. Somorjai and M. A. Van Hove, "Adsorbed Monolayers on Solid Surfaces," Structure and Bonding 38, 1 (1979).
12. J. B. Pendry, "Low Energy Electron Diffraction," Academic Press (New York), 1974.
13. M. A. Van Hove and S. Y. Tong, "Surface Crystallography by LEED," Springer (Heidelberg), 1979.
14. M. Henzler, Surf. Sci. 19, 159 (1970); G. E. Laramore, J. E. Houston and R. L. Park, J. Vac. Sci. Technol. 10, 196 (1973).

15. J. E. Houston and R. L. Park, Surf. Sci. 21, 209 (1970); G. Ertl and J. Küppers, Surf. Sci. 21, 61 (1970); H. Jagodzinski, D. Wolf, and W. Moritz, Surf. Sci. 77, 223, 249, 265 and 283 (1978); M. G. Lagally, in "Chemistry and Physics of Solid Surfaces," Vol. III, ed., R. Vanselow, Springer (Berlin) 1982.

16. G. Ertl and D. Schillinger, J. Chem. Phys. 66, 2569 (1977).

17. J. C. Bertolini and B. Tardy, Surf. Sci. 102 (1981) 131.

18. J. P. Biberian and M. A. Van Hove, in "Vibrations at Surfaces," eds. R. Caudano, J.-M. Gilles and A. A. Lucas, Plenum (New York) 1982; J. P. Biberian and M. A. Van Hove, Surf. Sci., in press.

19. W. Erley, H. Wagner, H. Ibach, Surf. Sci. 80, 612 (1979).

20. A. M. Bradshaw, F. M. Hoffman, Surf. Sci. 72, 513 (1978).

21. L. H. Dubois, G. A. Somorjai, Surf. Sci. 91, 512 (1980).

22. H. Froitzheim, H. Hopster, H. Ibach, S. Lehwald, Appl. Phys. 13, 147 (1977).

23. H. Hopster, H. Ibach, Surf. Sci. 77, 109 (1978).

24. G. E. Thomas and W. H. Weinberg, J. Chem. Phys. 70 (1979), 1437.

25. B. Sexton, Chem. Phys. Lett. 63 451 (1979).

26. S. Andersson, Surf. Sci. 89 477 (1979).

27. F. Jona, K. O. Legg, H. D. Shih, D. W. Jepsen and P. M. Marcus, Phys. Rev. Lett. 40, 1466 (1978).

28. R. Whyman, J.C.S. Chem. Comm., 1194 (1970).

29. W. P. Griffith, A. J. Wickam, J. Chem. Soc. A, 8344 (1969).

30. L. A. Hanlan, G. A. Ozin, J. Amer. Chem. Soc. 96, 6324 (1974).

31. J. G. Roth, M. J. Dignam, Can. J. Chem. 54, 1388 (1976).

32. M. Moskovitz, J. W. Hulse, Surf. Sci. 78, 397 (1978).

33. M. Scheffler, Surf. Sci. 78, 397 (1978).

34. G. Blyholder, J. Phys. Chem. 68, 528 (1977).

35. A. C. Yang, C. W. Garland, J. Phys. Chem. 61, 1504 (1957).

36. N. Sheppard, T. T. Nguyen in, Advances in Infrared and Raman Spectroscopy, 5, R.J.H. Clark, R. E. Hester, Eds., Heydon and Sons, (London), 1978, p. 67 and refs. therin.

37. R. J. Koestner, M. A. Van Hove and G. A. Somorjai, Surf. Sci. 107, 439 (1981).

38. S. Andersson and J. B. Pendry, Surf. Sci. 71, 75 (1978); J. Phys. C13, 3547 (1980).

39. S. Y. Tong, A. Maldonado, C. H. Li and M. A. Van Hove, Surf. Sci. 94, 73 (1980).

40. M. A. Van Hove and R. J. Koestner, Proc. Conf. on Determination of Surface Structure by LEED, Plenum (New York) 1982 (to appear).

41. E. Zanazzi and F. Jona, Surf. Sci. 62, 61 (1977).

42. J. B. Pendry, J. Phys. C13, 937 (1980).

43. P. Chini, V. Longoni and V. G. Albano, Adv. Organomet. Chem. 14, 285 (1976).

44. M. A. Van Hove, R. J. Koestner and G. A. Somorjai, to be published.

45. D. G. Castner, B. A. Sexton, G. A. Somorjai, Surf. Sci. 71, 519 (1978).

46. P A. Thiel, E. D. Williams, J. T. Yates, Jr., W. H. Weinberg, Surf. Sci. 84, 54 (1979).

47. B. A. Sexton, G. A. Somorjai, J. Catal. 46, 167 (1977).

48. The Rh(111) surface is catalytically active for Fischer-Tropsch synthesis, but at pressures above 1 atm.: D. G. Castner, R. L. Blackadar, G. A. Somorjai, J. Catal. 66, 257 (1980).

49. P. A. Thiel, J. T. Yates, Jr., W. H. Weinberg, Surf. Sci. 82, 22 (1979).

50. P. Skinner, M. W. Howard, I. A. Oxton, S F. A. Kettle, D. P. Powell, N. Sheppard, to be published.

51. E. L. Garfunkel, J. E. Crowell and G. A. Somorjai, J. Phys. Chem. 86 (1982) 310.

52. E. L. Garfunkel and G. A. Somorjai, Surf. Sci., 115, 441 (1982).

53. C. T. Campbell, G. Ertl, H. Kuipers, and J. Segner, Surf. Sci. 107, 207 (1981).

54. M. E. Dry, T. Shingles, L. J. Boshoff and G. J. Oosthuizen, J. Cat. 15, 190 (1969).

55. T. P. Wilson, W. J. Bartley and P. C. Ellgen, to be published.

56. L. H. Dubois, D. G. Castner, and G. A. Somorjai, J. Chem. Phys. 72, 5234 (1980).

57. R. J. Koestner, M. A. Van Hove and G. A. Somorjai, to be published.

58. See, for example, T. Shimanouchi, Tables of Molecular Vibrational Frequencies, consolidated Vol. 1, U.S. Dept. of Commerce publ. NSROS-NBS 39 (1972).

59. E. L. Muetterties, Bull. Soc. Chim. Belg. 84, 959 (1975).

60. E. L. Muetterties, T. N. Rhodin, E. Band, C. F. Brucker and W. R. Pretzer, Chem. Rev. 79, 91 (1979).

61. J. E. Demuth and H. Ibach, Surf. Sci. 78, L238 (1978).

62. T. Hazttori and R. L. Burwell, Jr., J. Phys. Chem. 83, 241 (1979).

63. H. Ibach, H. Hopster and B. Sexton, Appl. Surf. Sci. 1, 1 (1977); H. Ibach and S. Lehwald, J. Vac. Sci. Technol. 15, 407 (1978).

64. L. L. Kesmodel, L. H. Dubois and G. A. Somorjai, J. Chem. Phys. 70, 2180 (1979).

65. M. Salmeron and G. A. Somorjai, J. Phys. Chem., 86, 341 (1982).

66. W. Ho, J. DiNardo and E. W. Plummer, J. Vac. Sci. Techn. 17, 134 (1980).

67. K. Christmann, R. J. Behm, G. Ertl, M. A. Van Hove and W. H. Weinberg, J. Chem. Phys. 70, 4168 (1979).

68. A. M. Baro, H. Ibach and H. D. Bruchmann, Surf. Sci. 88, 384 (1979).

69. R. J. Koestner, J. C. Frost, P. C. Stair, M. A. Van Hove and G. A. Somorjai, Surf. Sci. 116, 85 (1982).

70. B. A. Sexton, Surf. Sci. 102, 271 (1981).

71. B. A. Sexton, Surf. Sci. 88, , 299 (1979).

72. K. Nakamoto, Infrared and Raman Spectro of Inorganic and Coordination Compounds, Wiley, (New York), 1978.

73. J. L. Gland and B. A. Sexton, J. Catal. 68, 286 (1981).

74. L. H. Dubois, G. A. Somorjai and P. K. Hansma, Appl. Surf. Sci. 6, 173 (1980).

75. R. M. Kroeker, W. C. Kasha, P. K. Hansma, J. Catl. 57, 72 (1979); 61, 87 (1980).

76. P. K. Hansma, D. A. Hickson, J. A. Schwarz, J. Catal. 48, 234 (1977); W. M. Bowser, W. H. Weinberg, Surf. Sci. 64, 377 (1977).

77. D. G. Walmsley, R. B. Floyd, W. E. Timms, Sol. St. Commun. 22, 497 (1977); M. F. Muldoon, R. A. Dragoset, R. V. Coleman, Phys. Rev. B20, 416 (1979).

78. P. K. Hansma, Phys. Rep. 30, 145 (1977).

79. L. H. Little, Infrared Spectroscopy of Adsorbed Species, Academic Press, (London), 1966.

80. J. T. Yates, Jr., T. M. Duncan, S. D. Worley, R. W. Vaughn, J. Chem. Phys. 70, 1219 (1979).

Table I. Metal carbonyl structures and CO stretching frequencies for surfaces and for clusters. The frequencies (measured by HREELS or IR) are classified qualitatively according to the customary adsorption site assignment, for comparison with the site determined by LEED. For clusters the stars indicate the range in which CO stretching frequencies fall. The CO bond length (d_{CO}) and metal-C bond length (d_{MC}) are indicated, together with the corresponding metal-C layer spacing ($d_{\perp MC}$) and an effective carbon radius (r_C) obtained by subtracting the bulk or cluster metallic radius from the metal-C bond length.

		CO stretching frequency (cm^{-1})			Site from	d_{CO}	$d_{\perp MC}$	d_{MC}	r_C
		hollow	bridge	top	LEED	(Å)	(Å)	(Å)	(Å)
			1850	2000					
Surfaces									
Ni(100)+(2x2)CO				2069	top	1.15	1.76	1.76	.52
Cu(100)+c(2x2)CO				2079-2089	top	1.13	1.90	1.90	.62
Pd(100(+(2$\sqrt{2}$x$\sqrt{2}$)R45°2CO				1903-1949	bridge	1.15	1.36	1.93	.56
Rh(111)+($\sqrt{3}$x$\sqrt{3}$)R30°CO				2020	top	1.07	1.95	1.95	.61
Rh(111)+(2x2)3CO			1870	2070	top +	1.15	1.87	1.94	.60
					bridge	1.15	1.52	2.03	.69
Free CO				2143		1.15			
Organometallic Clusters									
Ni-Metal	top			*		1.01-1.16		1.75-1.89	.56-.72
	bridge		*			1.07-1.17		1.82-1.91	.65-.74
Rh-metal	top			*		1.09-1.17		1.82-1.91	.43-.50
	bridge		*			1.14-1.17		2.00-2.09	.58-.59
	hollow	*				1.15-1.20		2.17-2.23	.78-.82

Table II. Vibrational modes for the metastable (2x2) C_2H_2 (C_2D_2) species observed on Rh(111) at <270 K (all frequencies in cm^{-1})

C_2H_2 (C_2D_2) / Rh(111)	Assignments
3085 (~ 23023) w 2984 (2230) m	C-H (C-D) stretch
a.	C-C stretch
887 (686) m 706 (565) m	C-H (C-D) bend
323 (300) w	Rh-C stretch

Intensity: s = strong m = medium w = weak

a. Small broad peak in the 1300-1400 cm^{-1} region is observed in several spectra.[56]

Table III. Bond distances and angles for ethylidyne species in clusters and at surfaces, compared with corresponding data for ethane, ethylene and acetylene. The C-C bond length (d_{CC}) and the metal-C bond length (d_{MC}) are indicated, together with the bulk or cluster metallic radius, which is subtracted from d_{MC} to yield the carbon covalent radius (r_C). Also included is the C-C-M or C-C-H bond angle.

Ethylidyne Species	d_{CC}(Å)	d_{MC}	r_M	r_C	α[°]
$Co_3(CO)_9CCH_3$	1.53(3)	1.90(2)	1.24	0.66	131
$H_3Ru_3(CO)_9CCH_3$	1.51(2)	2.08(1)	1.42	0.66	128
$H_3Os_3(CO)_9CCH_3$	1.51(2)	2.08(1)	1.42	0.66	128
$[P(C_6H_5)_3]Co_3(CO)_8CCH_3$	1.50(2)	1.91(2)	1.25	0.66	131
$[\pi\text{-}C_6H_3Me_3]Co_3(CO)_6CPh$	1.48(2)	1.89(2)	1.23	0.66	132
$[\pi\text{-}C_8H_8]Co_3(CO)_6CPh$	1.48(2)	1.89(2)	1.23	0.66	132
$Rh(111)+(2x2)CCH_3$	1.45(5)	2.03(4)	1.34	0.69	130
$Pt(111)+(2x2)CCH_3$	1.50(5)	2.00(4)	1.39	0.61	127
$H_3C - CH_3$	1.54			0.77	110
$H_2C = CH_2$	1.33			0.67	122
HC CH	1.20			0.60	180

FIGURE CAPTIONS

Figure 1. Schematic diagram of the high resolution electron energy loss spectrometer used in our studies. The dispersive elements are 127° cylindrical sectors.

Figure 2. Electron diffraction patterns for Pt(111) at different electron energies, at normal incidence. With increasing energy the diffraction spots converge toward the specular reflection spot, here hidden by the crystal sample.

Figure 3. Experimental I-V (intensity vs. voltage or energy) curves for electron diffraction from a Pt(111) surface. Beams are identified by different labels (h,k) representing reciprocal lattice vectors parallel to the surface. An incidence angle of 4° from the surface normal is used.

Figure 4. Vibrational spectra of CO chemisorbed on Rh(111) at 300 K as a function of CO exposure. Both the 480 and 1990 cm^{-1} losses shift with increasing surface coverage.

Figure 5. Vibrational spectra of CO chemisorbed on Rh(111) at 300 K as a function of background CO pressure. The loss above 2000 cm^{-1} shifts to a limiting value of 2070^{-1} while the peak at 1870 cm^{-1} increases in intensity at a constant frequency.

Figure 6. LEED patterns for CO adsorption on Rh(111). a) clean Rh(111); b) $(\sqrt{3}x\sqrt{3})R30°$ pattern for 1/3 monolayer of CO; c) "split (2x2)" pattern for between 1/3 and 3/4 monolayer of CO; d) (2x2) pattern for 3/4 monolayer of CO.

Figure 7. Comparison between experimental (thick) and theoretical (thin) I-V curves for Rh(111)+$(\sqrt{3}x\sqrt{3})R30°$ CO at normal incidence for four independent beams.

Figure 8. Surface structure of Rh(111)+(2x2)3CO (b) compared with that of Rh(111)+($\sqrt{3}$x$\sqrt{3}$)R30°CO (a). Dark circles represent CO molecules seen end-on against the close-packed substrate (large open circles). The distance between nearest CO molecules in this projection is about 3.1Å.

Figure 9. Vibrational spectra of the saturation coverage of CO chemisorbed on Pt(111) at 300K as the amount of preadsorbed potassium is increased.

Figure 10. Vibrational spectra of CO chemisorbed on Pt(111) predosed with 0.3 monolayers of potassium as the substrate temperature in changed (i.e., CO coverage).

Figure 11. HREELS spectra of chemisorbed acetylene on Rh(111); bottom (2x2)-C_2H_2; middle (2x2)-C_2D_2; top c(4x2)-C_2H_2+H.

Figure 12. HREELS spectra of chemisorbed ethylene on Rh(111); bottom (2x2) from C_2H_4 chemisorption; middle c(4x2) from C_2H_4 chemisorption; top (2x2) from C_2D_4 chemisorption.

Figure 13. CH (CD) species can be formed on Rh(111) by heating chemisorbed C_2H_2 or C_2D_2 to 450 K.

Figure 14. Comparison of the vibrational spectra for ethylene chemisorbed on Pt(111) and Rh(111). A discussion of the similarities between acetylene and ethylene chemisorption on Rh(111) and Pt(111) is presented in Ref. 56.

Figure 15. Propylidyne on Pt(111).

Figure 16. Butylidyne on Pt(111).

Figure 17. Butylidyne on Pt(111) in the (2$\sqrt{3}$x2$\sqrt{3}$)R30° strcuture, using Van der Waals radii for each atom (top view), or emphasizing the carbon skeleton (bottom view).

Figure 18. Cross sectional view of the model supported metal catalyst. When a small quantity of rhodium is evaporated onto oxidized aluminum it agglomerates into small particles. For an average Rh thickness of 4 Å, the Rh particles are 20 to 30 Å in diameter and the oxidized substrate is similar to λ alumina.

Figure 19. The spectrum from HREELS for the aluminum oxide support is shown in the lowest trace. The broad band, asymmetric to lower wavenumbers and centered around 960 cm^{-1} is the aluminum oxide phonon band. The upper two traces show the vibrational spectra for two different amounts of rhodium evaporated onto the alumina support in $1x10^{-5}$ torr of CO (4 Å and 20 Å average Rh thicknesses).

Figure 20. Vibrational spectra taken by 3 different techniques for CO adsorbed on Rh particles supported on alumina. The infrared spectra (upper traces) are from the work of Yates, et al..[80] The high resolution of IR spectroscopy is evident. The inelastic electron tunneling spectrum (lower trace), taken from the work of Kroeker et al.,[75] shows the downshift in the CO stretching vibrations that are characteristic of tunneling spectroscopy and the relatively strong low frequency modes. The HREELS spectrum approximates an envelope of the CO stretching frequencies observed in the infrared spectra.

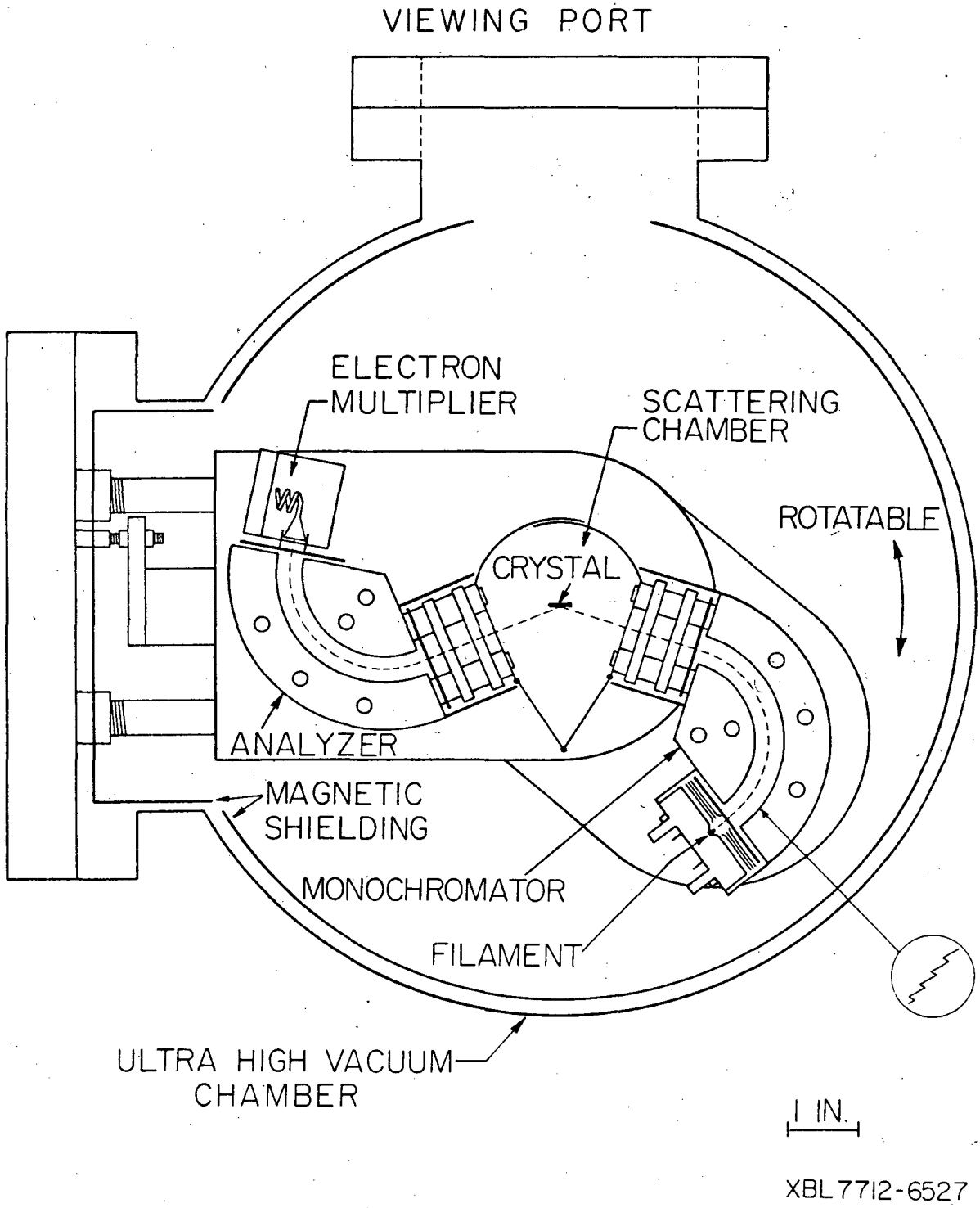
VIEWING PORT
ELECTRON MULTIPLIER
SCATTERING CHAMBER
ROTATABLE
CRYSTAL
ANALYZER
MAGNETIC SHIELDING
MONOCHROMATOR
FILAMENT
ULTRA HIGH VACUUM CHAMBER
1 IN.
XBL7712-6527

Fig. 1

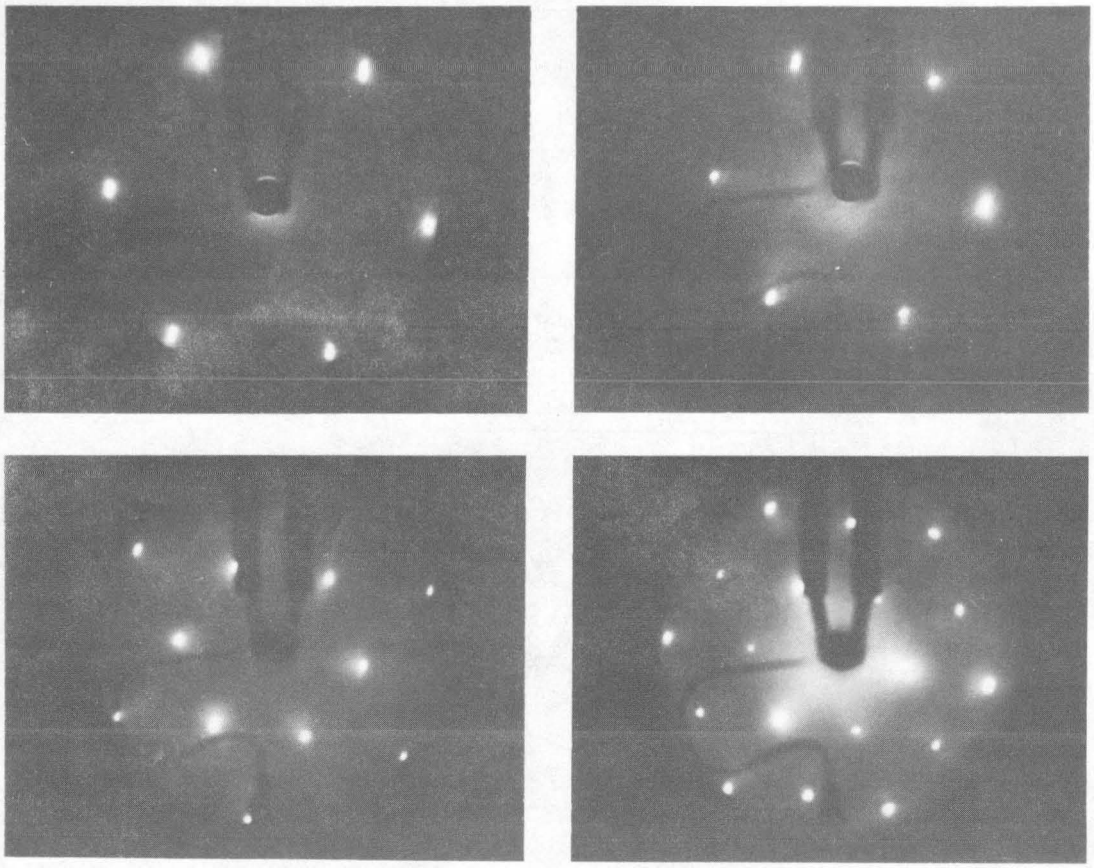

XBB 700-5685

Fig. 2

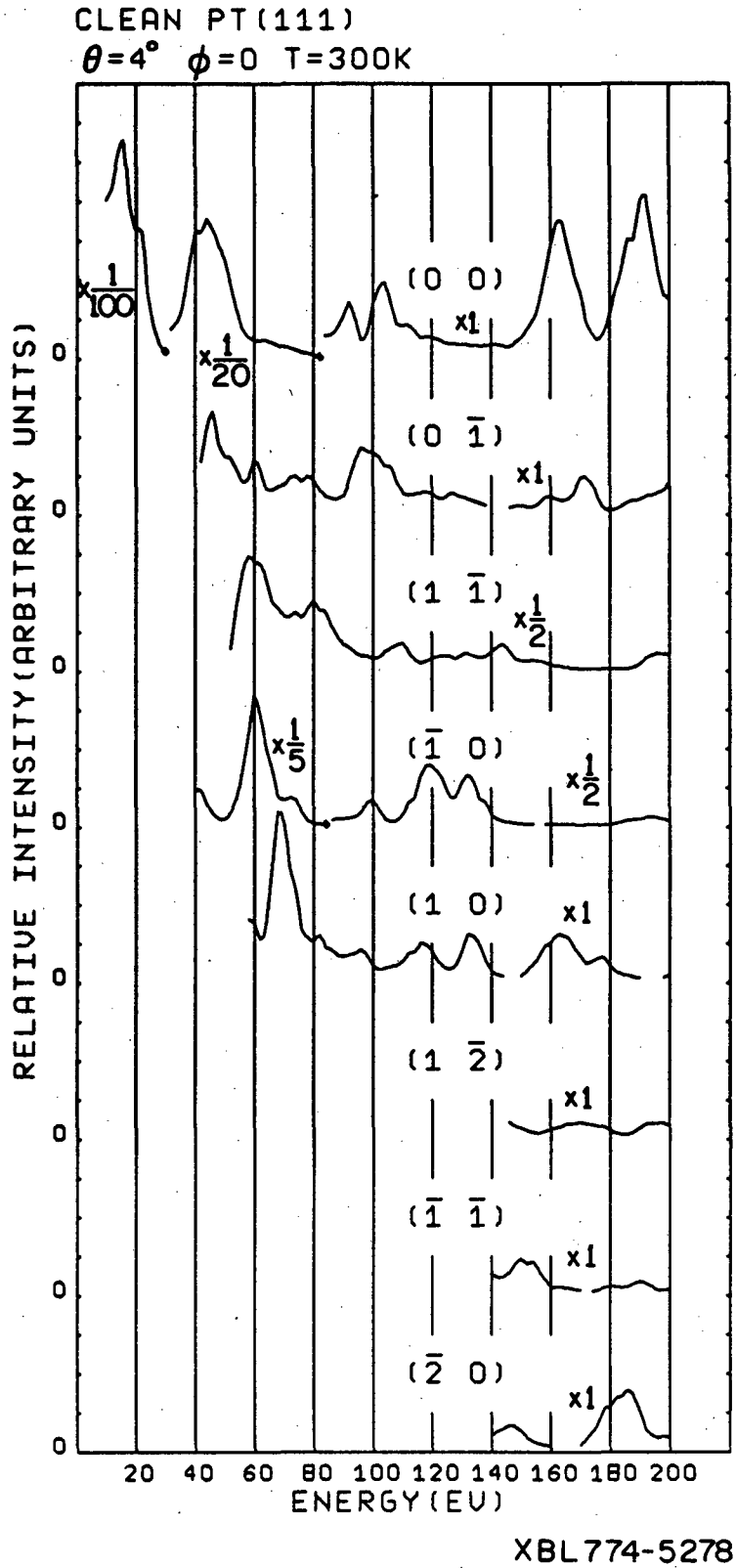
CLEAN PT(111)
θ=4° φ=0 T=300K
RELATIVE INTENSITY(ARBITRARY UNITS)
ENERGY(EV)
(0 0)
(0 1̄)
(1 1̄)
(1̄ 0)
(1 0)
(1 2̄)
(1̄ 1̄)
(2̄ 0)
x1/100
x1/20
x1/5
x1/2
x1
20 40 60 80 100 120 140 160 180 200
XBL774-5278

Fig. 3

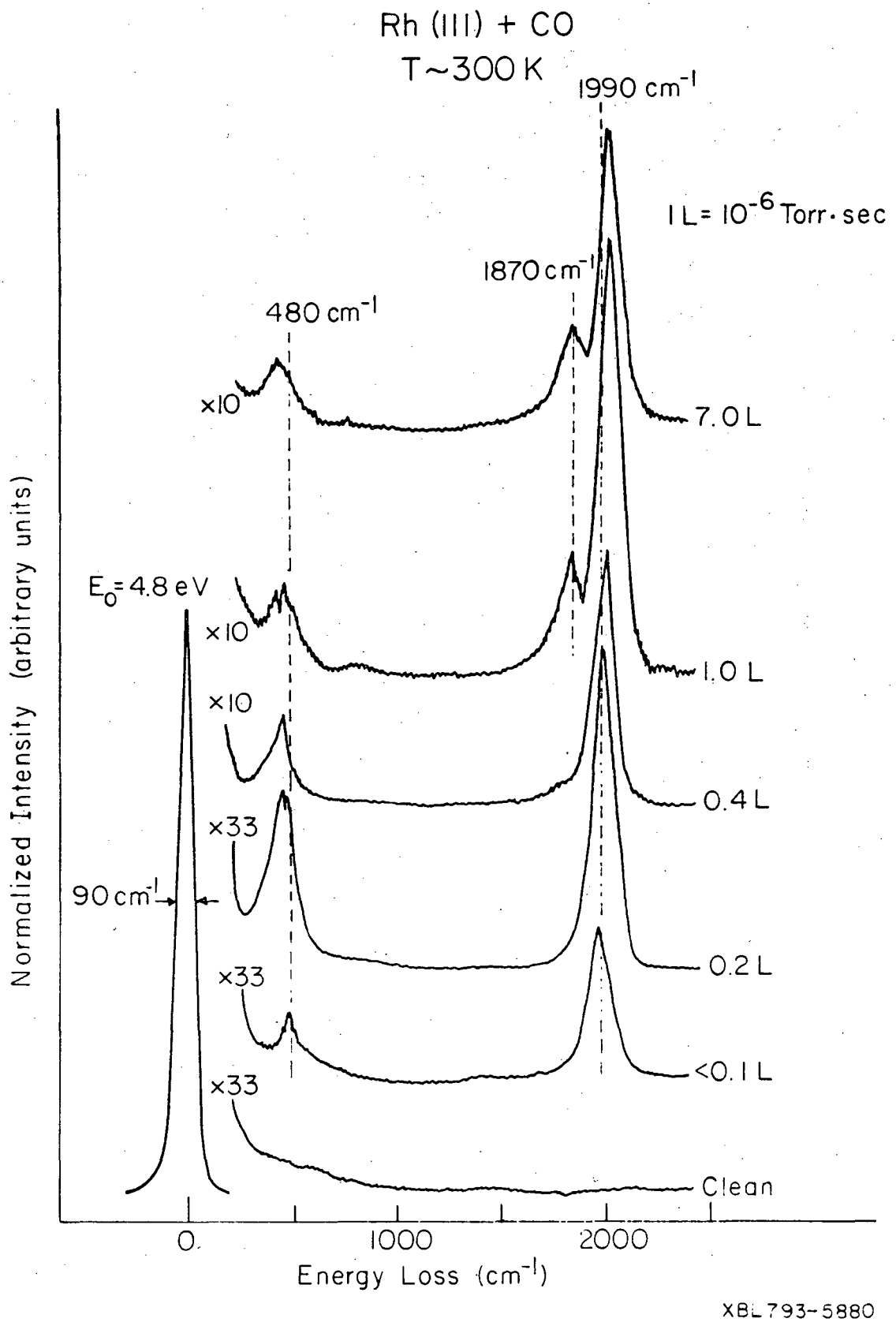
Rh (111) + CO
T~300 K
1990 cm⁻¹
1 L = 10⁻⁶ Torr·sec
1870 cm⁻¹
480 cm⁻¹
×10
7.0 L
E₀ = 4.8 eV
×10
1.0 L
×10
0.4 L
×33
90 cm⁻¹
0.2 L
×33
<0.1 L
×33
Clean
Normalized Intensity (arbitrary units)
0
1000
2000
Energy Loss (cm⁻¹)
XBL 793-5880

Fig. 4

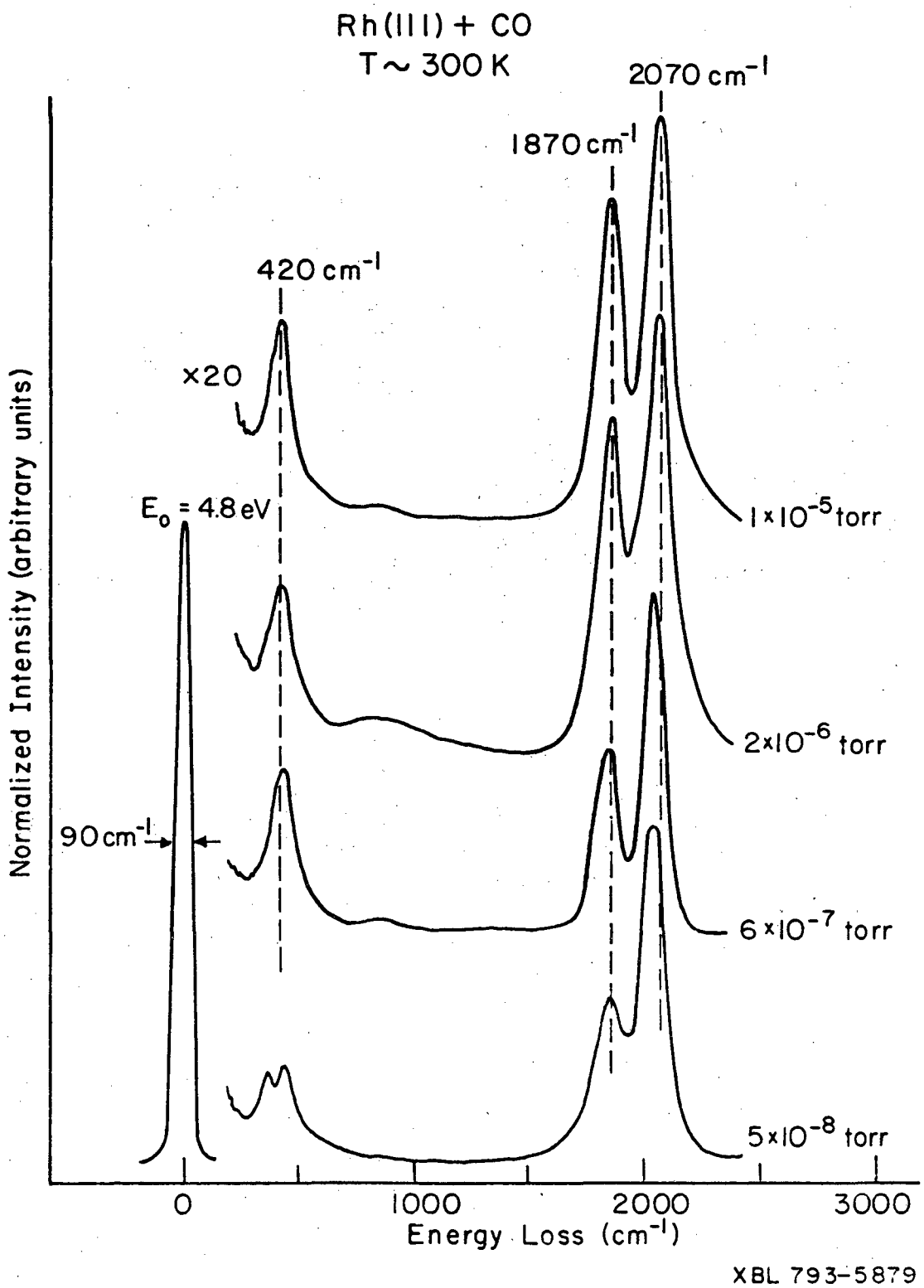
Rh(111) + CO
T ~ 300 K
2070 cm⁻¹
1870 cm⁻¹
420 cm⁻¹
×20
E₀ = 4.8 eV
90 cm⁻¹
1×10⁻⁵ torr
2×10⁻⁶ torr
6×10⁻⁷ torr
5×10⁻⁸ torr
Normalized Intensity (arbitrary units)
0
1000
2000
3000
Energy Loss (cm⁻¹)
XBL 793-5879

Fig. 5

CO/Rh(111)

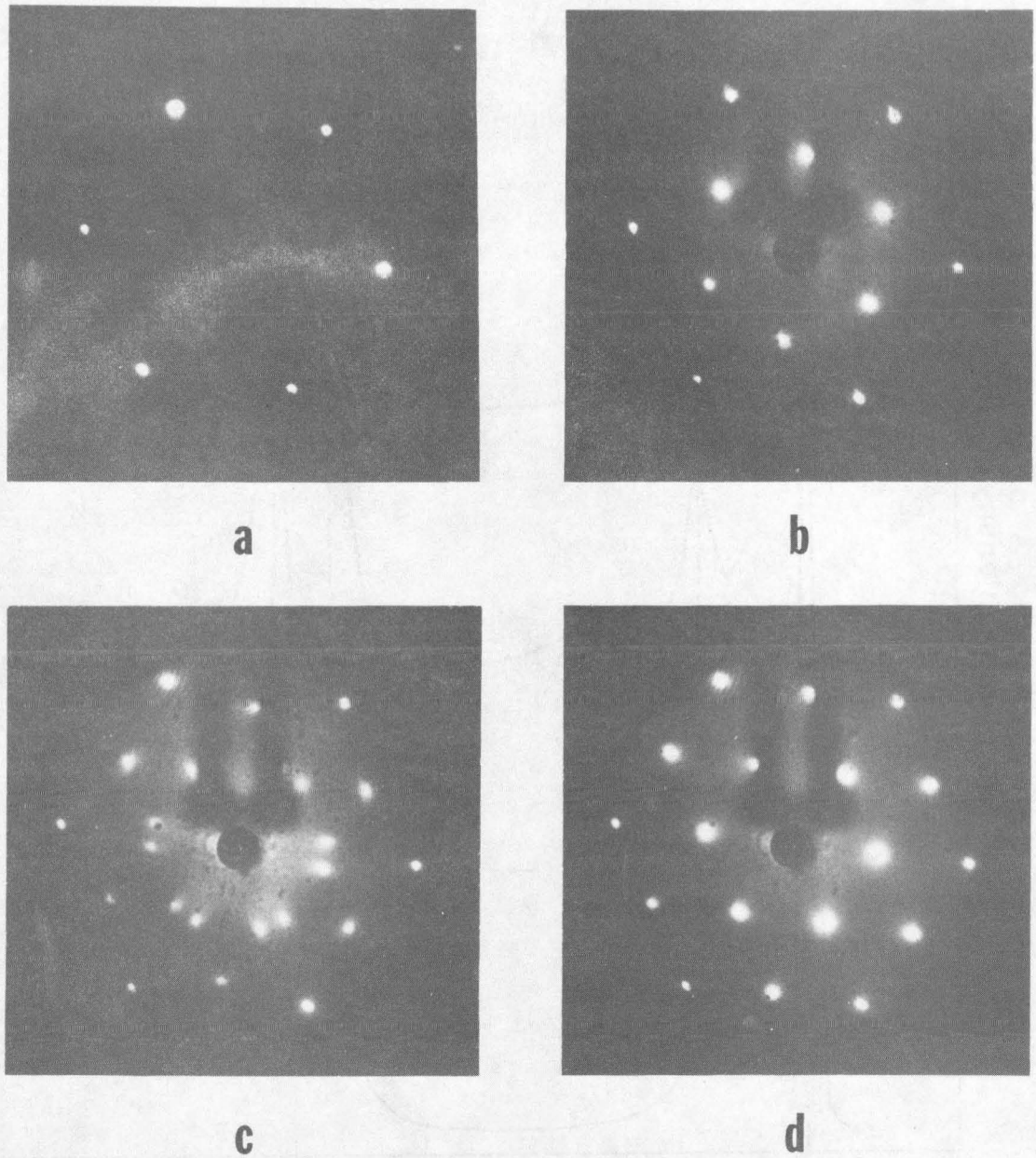

XBB 780-15407

Fig. 6

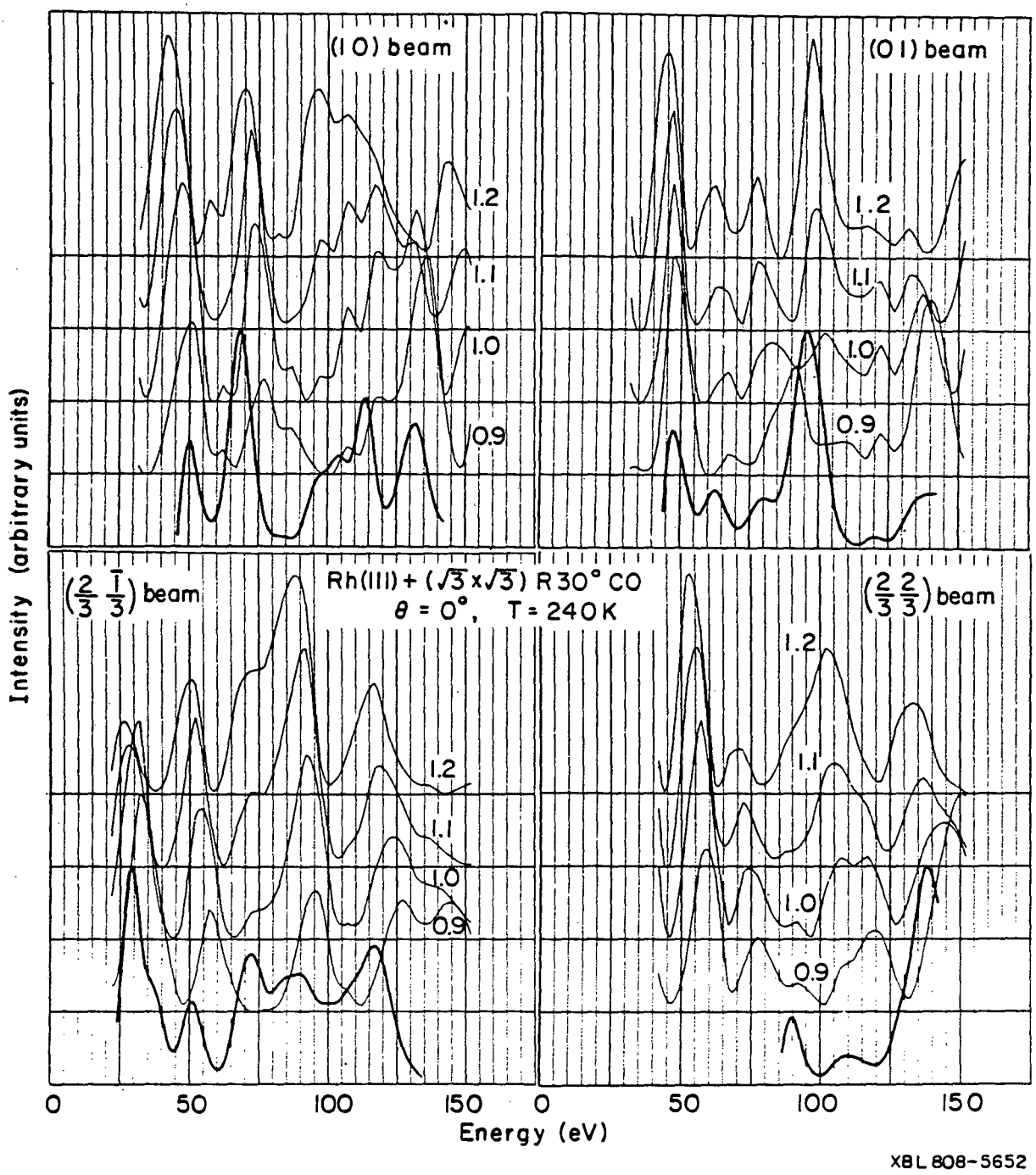
(1 0) beam
(0 1) beam
1.2
1.1
1.0
0.9
Rh(111) + (√3 x √3) R30° CO
θ = 0°, T = 240 K
(2/3 1̄/3) beam
(2/3 2/3) beam
Intensity (arbitrary units)
0
50
100
150
Energy (eV)
XBL 808-5652

Fig. 7

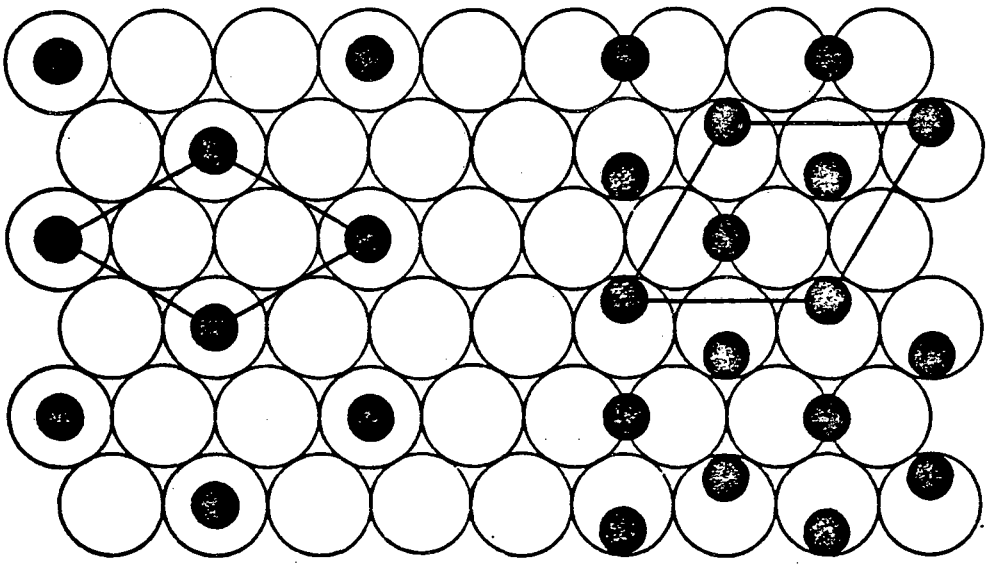

$(\sqrt{3} \times \sqrt{3})R30$ (2×2)

$\theta = 1/3$ $\theta = 3/4$

a. b.

XBL795-6248

Fig. 8

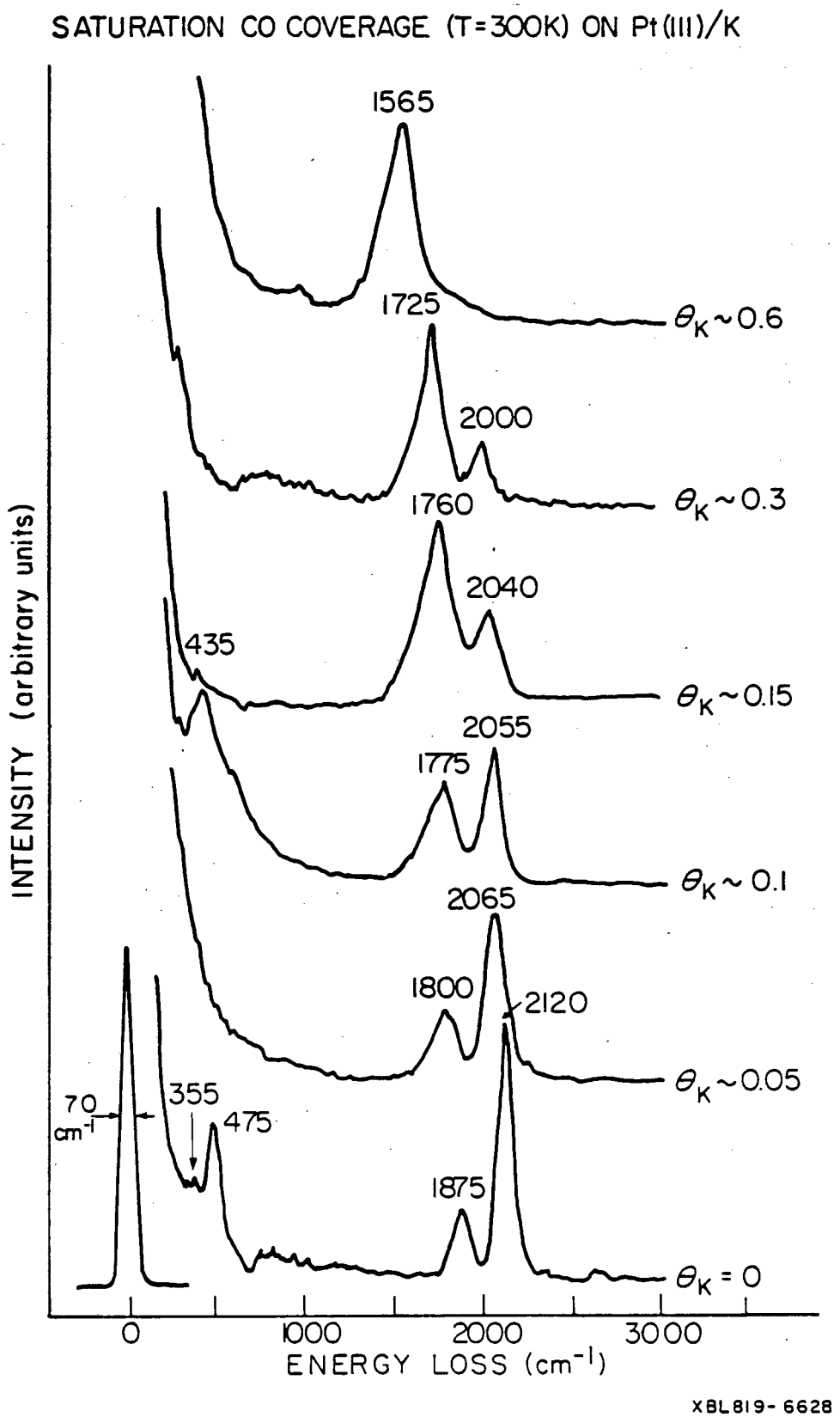
SATURATION CO COVERAGE (T=300K) ON Pt(111)/K
1565
1725
2000
1760
2040
435
2055
1775
2065
1800
2120
355
475
70
cm-1
1875
θK ~ 0.6
θK ~ 0.3
θK ~ 0.15
θK ~ 0.1
θK ~ 0.05
θK = 0
INTENSITY (arbitrary units)
0
1000
2000
3000
ENERGY LOSS (cm-1)
XBL819-6628

Fig. 9

CO COVERAGE DEPENDENCE ON Pt(111)/K (θ_K~0.3)

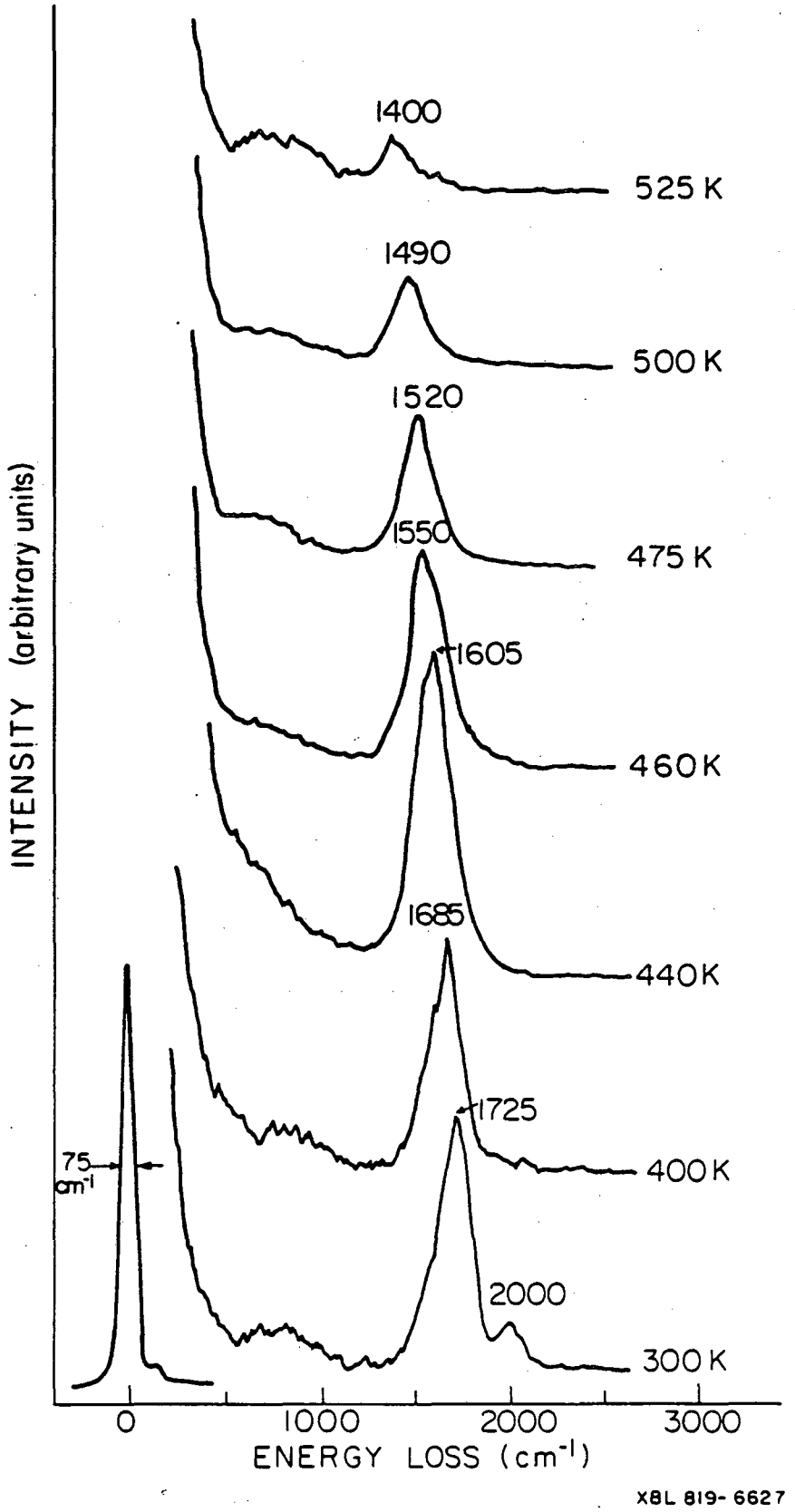

Fig. 10

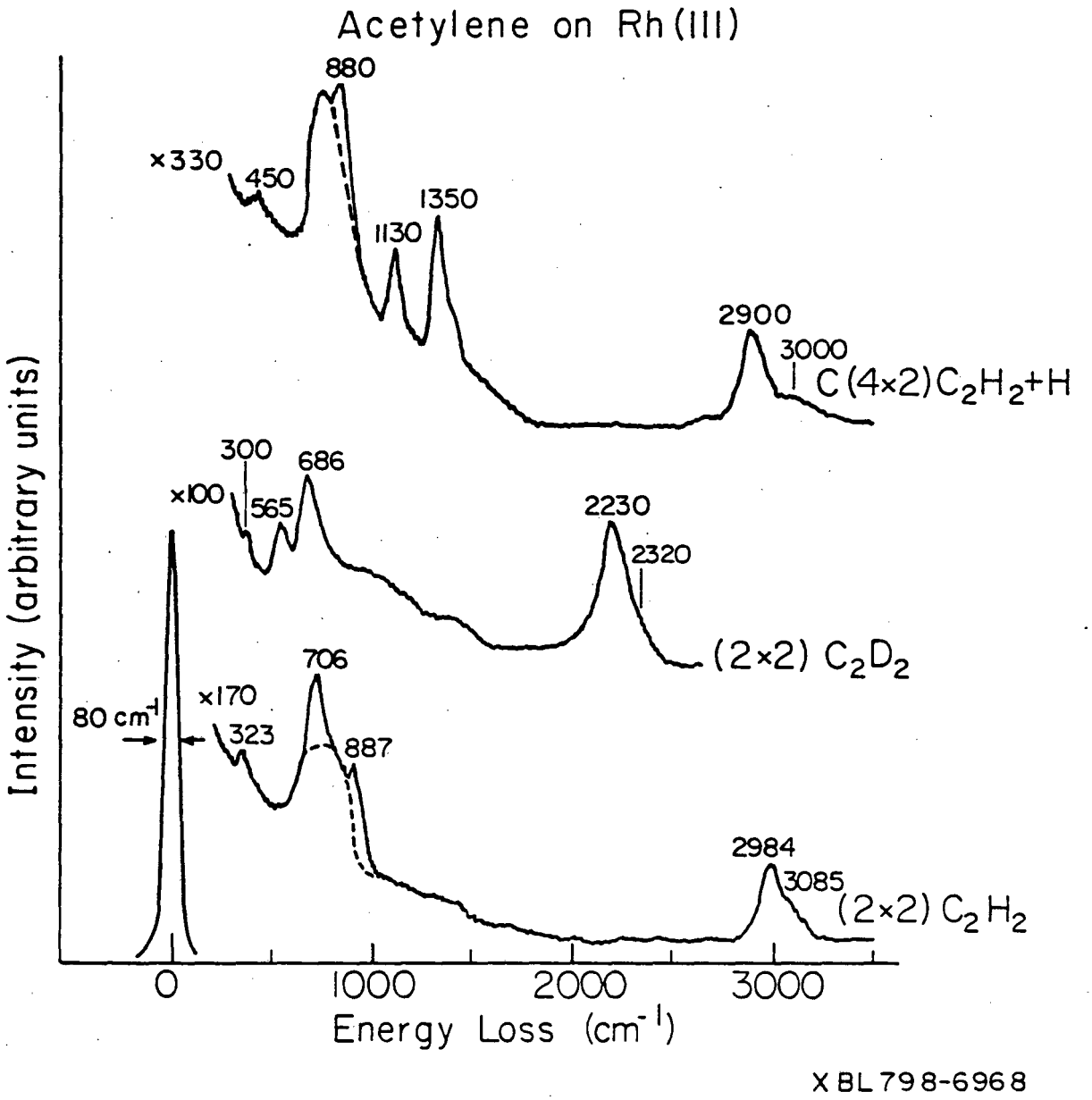
Acetylene on Rh(III)
880
×330
450
1350
1130
2900
3000
C(4×2)C2H2+H
300
686
×100
565
2230
2320
(2×2) C2D2
706
×170
80 cm-1
323
887
2984
3085
(2×2) C2H2
Intensity (arbitrary units)
0
1000
2000
3000
Energy Loss (cm-1)
XBL798-6968

Fig. 11

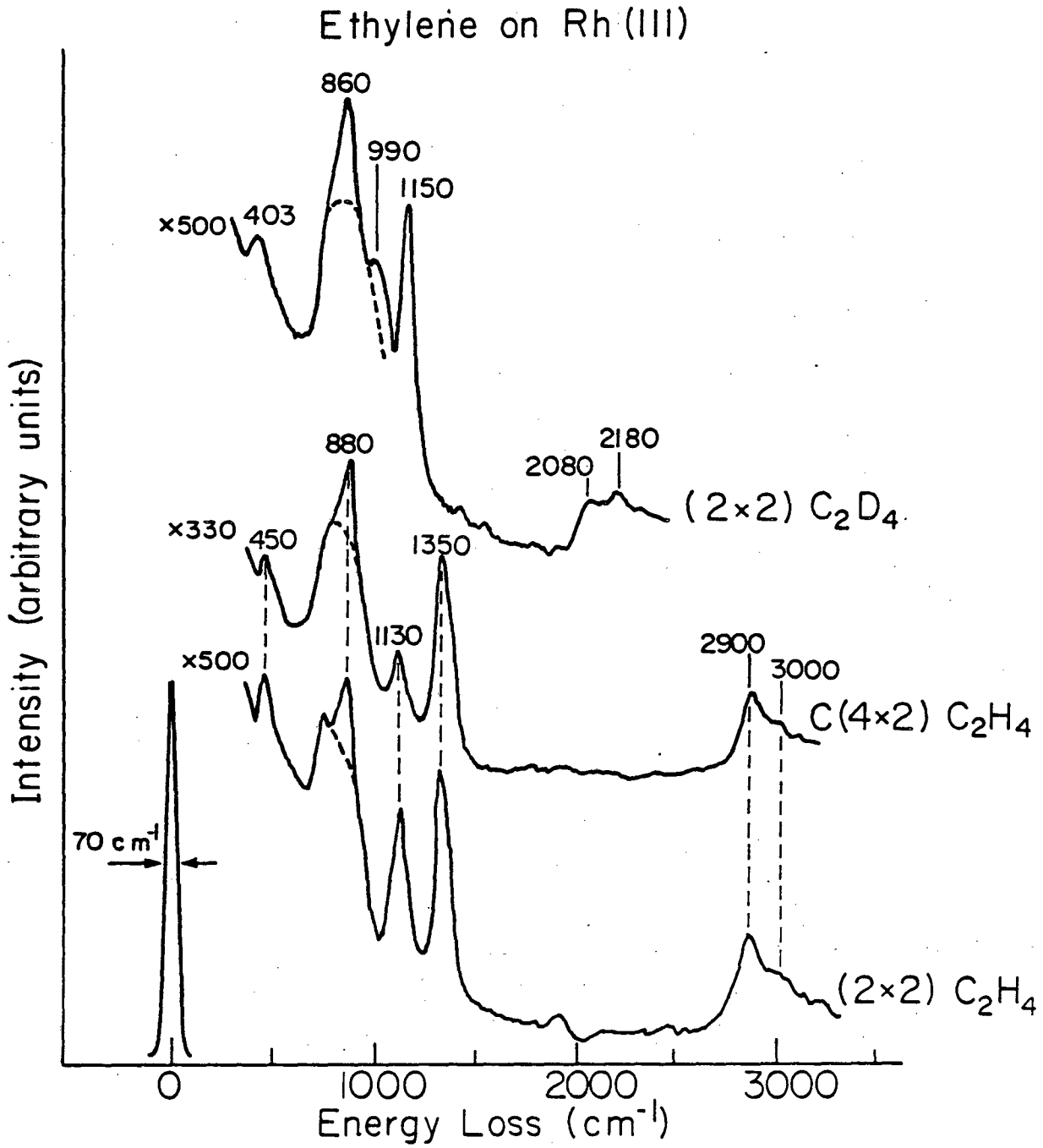

XBL798-6969

Fig. 12

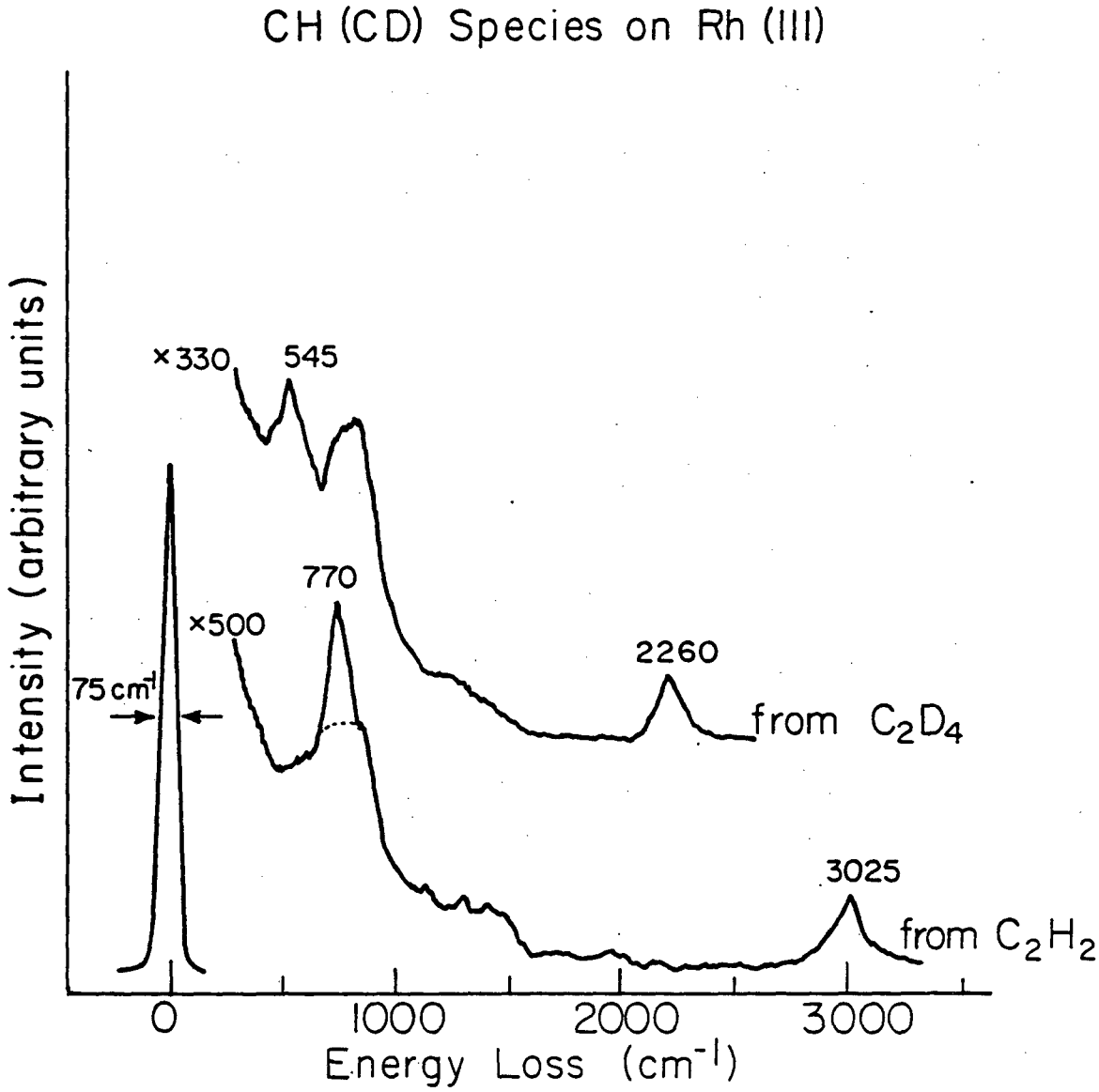
CH (CD) Species on Rh (III)
Intensity (arbitrary units)
×330
545
770
×500
2260
75 cm⁻¹
from C2D4
3025
from C2H2
0
1000
2000
3000
Energy Loss (cm⁻¹)
XBL 798-6970

Fig. 13

Ethylene Chemisorption on Rh and Pt

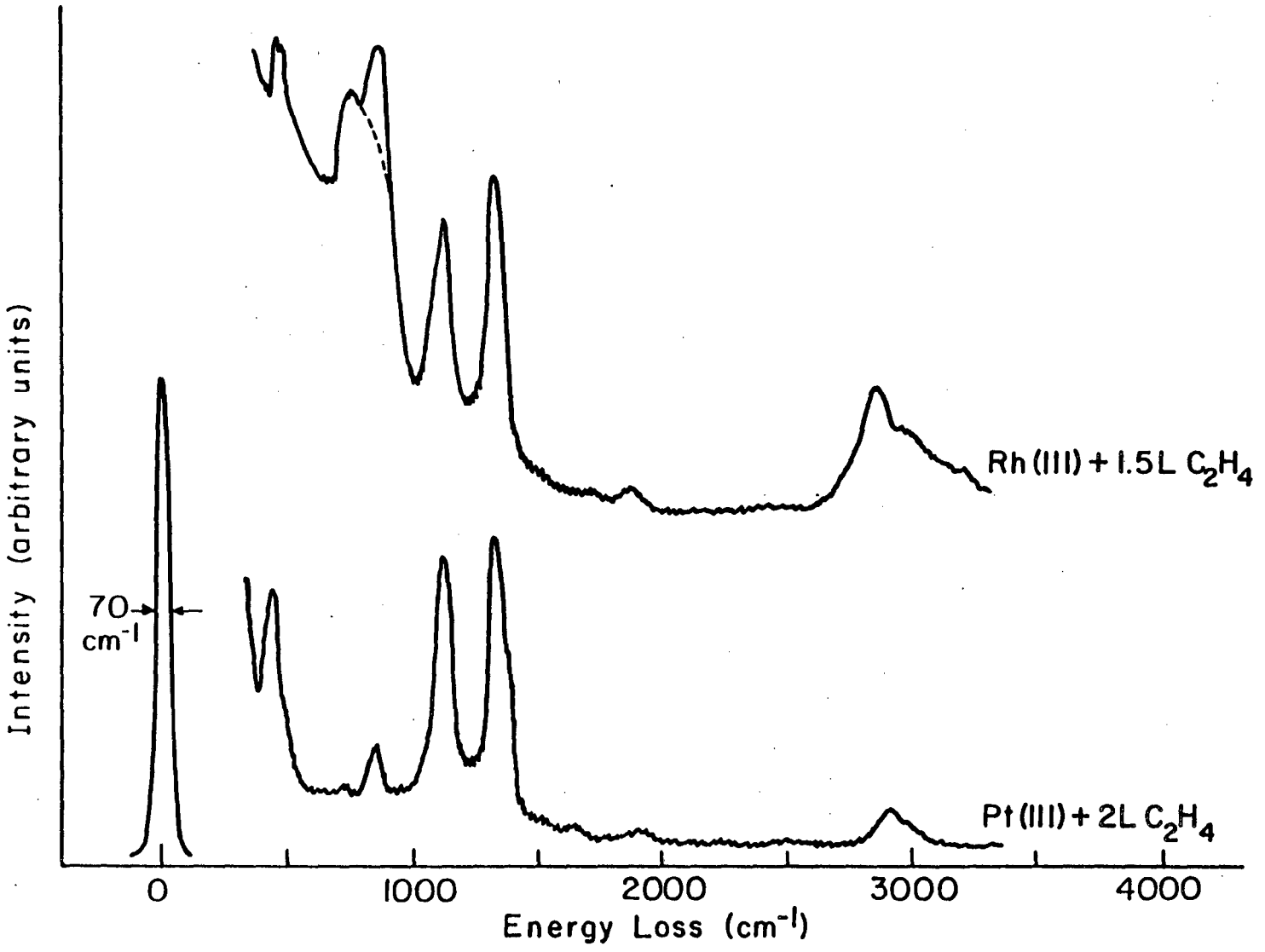

XBL 7911-7290

Fig. 14

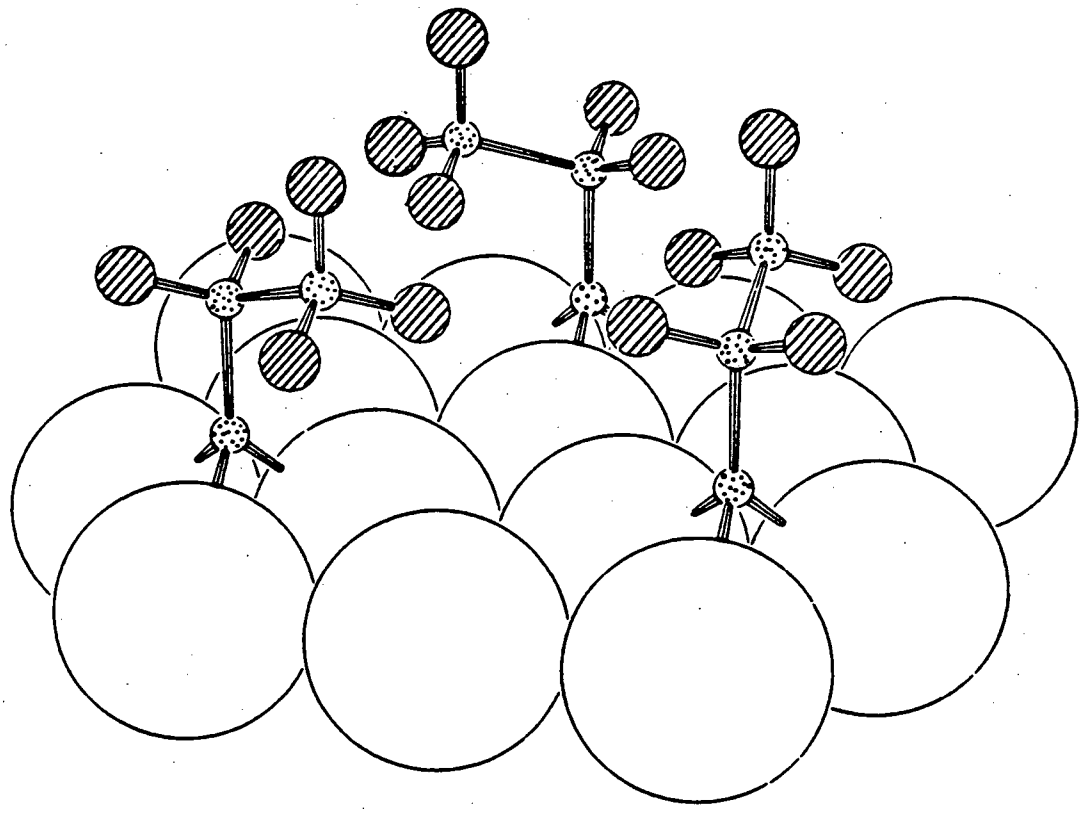

fcc (111) + C_3H_5 (propylidyne)

XBL 817-6065

Fig. 15

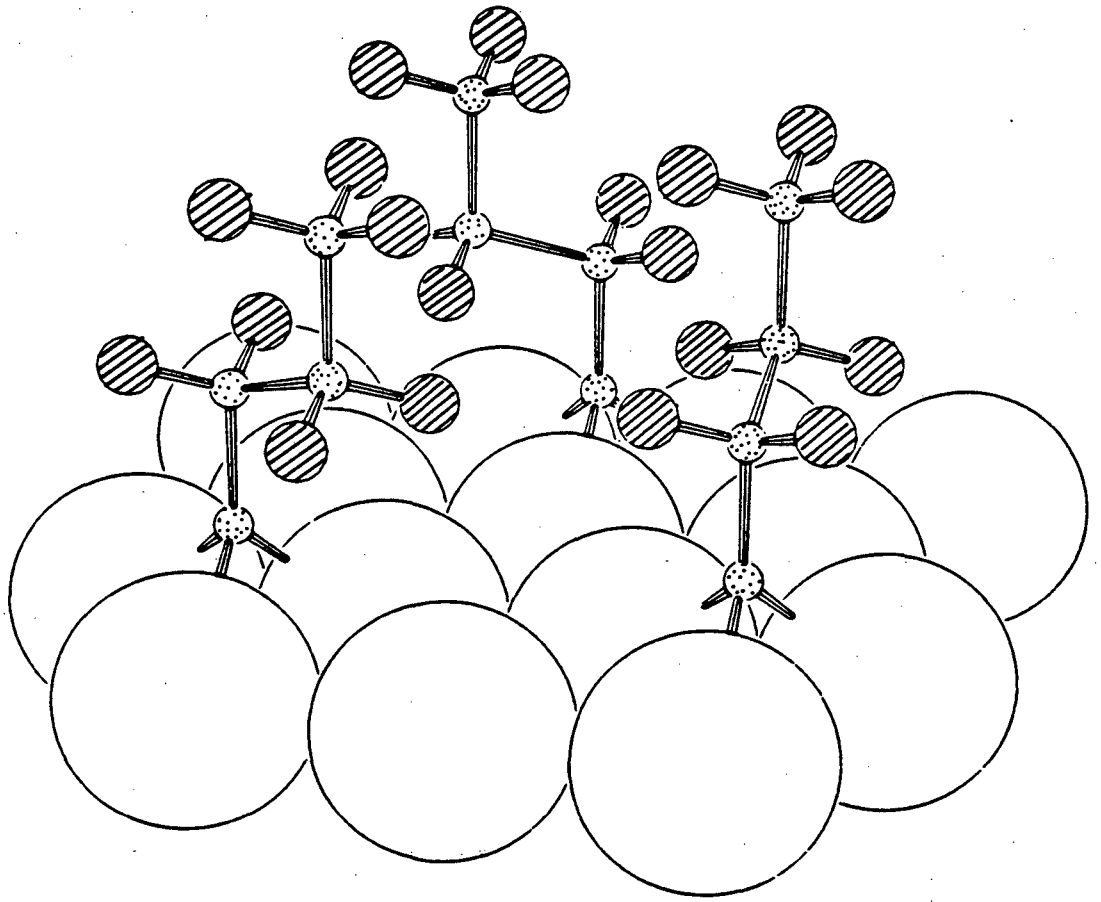

Pt(111) - $(2\sqrt{3} \times 2\sqrt{3})$ R 30° - 2 - C_4H_8

XBL 817-6134

Fig. 16

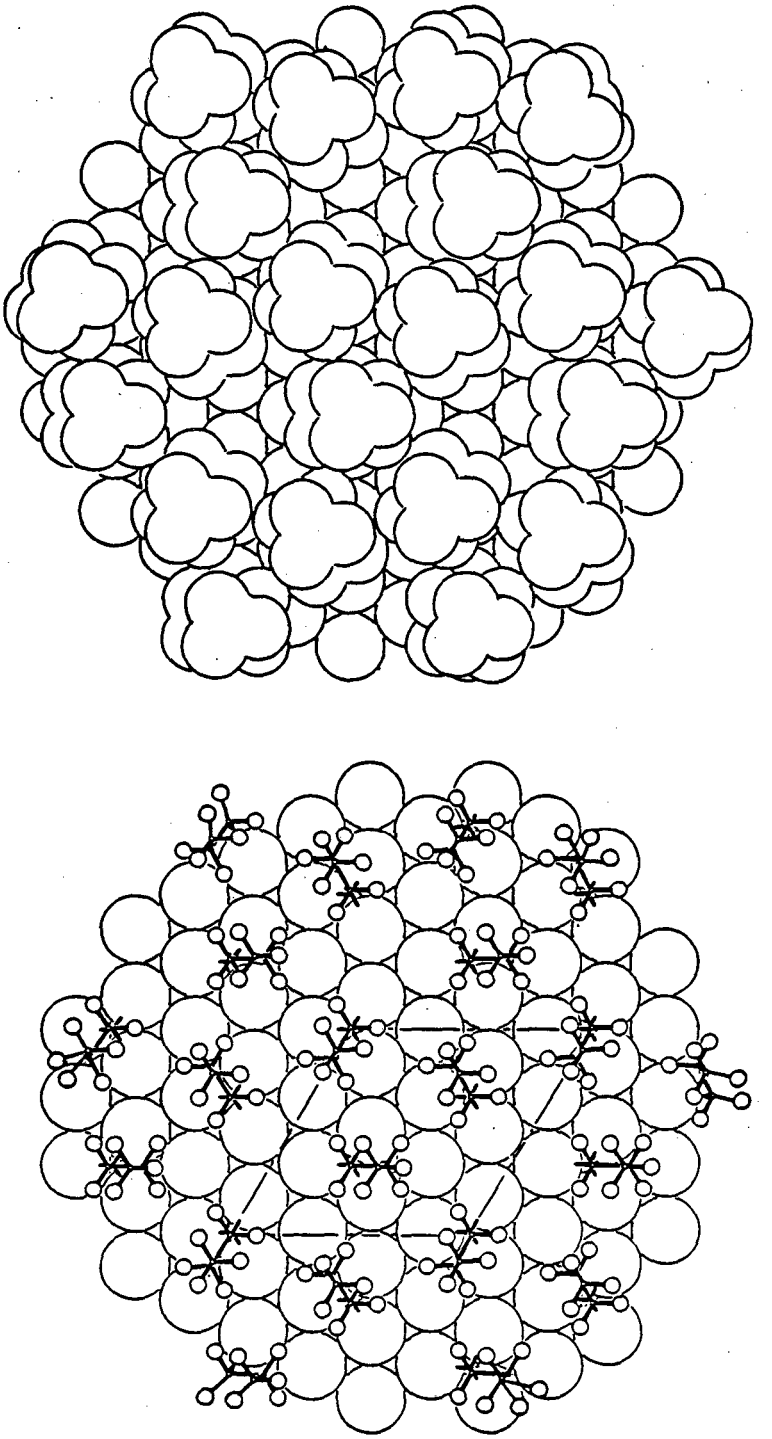

fcc(111) + $(2\sqrt{3}\times 2\sqrt{3})R30^\circ$ C_4H_7 (butylidyne)

XBL 813-5411

Fig. 17

Model Supported Rhodium Catalyst

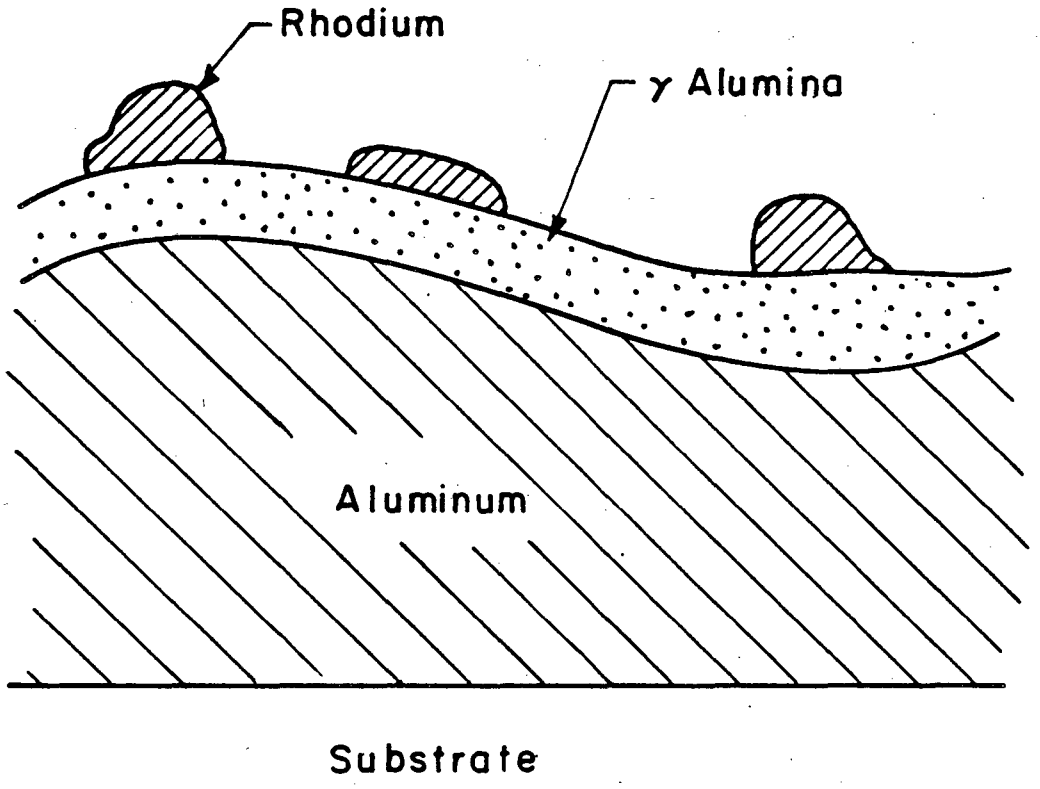

XBL 802-4730

Fig. 18

Vibrational Spectra of Model Catalysts

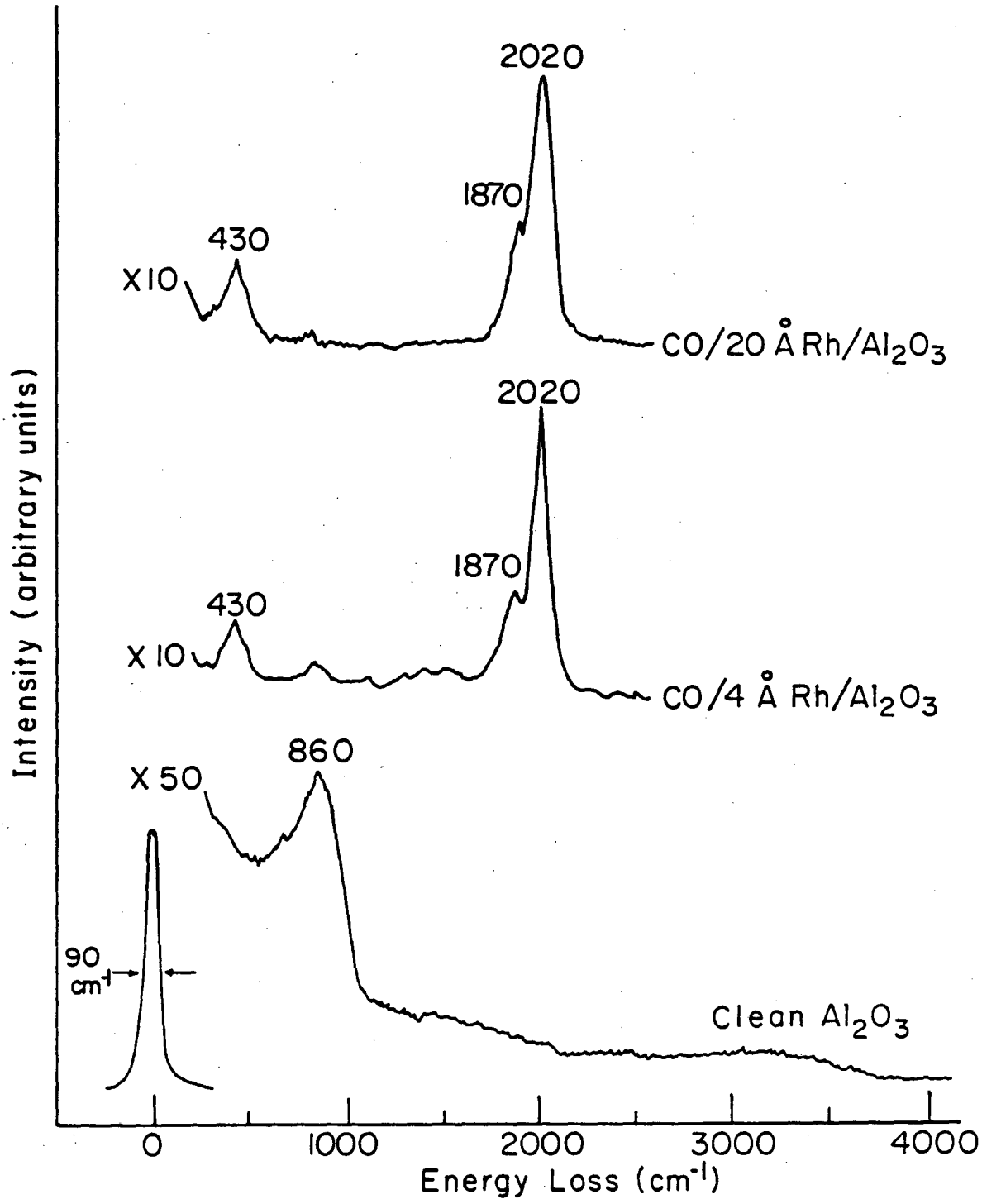

XBL802-4732

Fig. 19

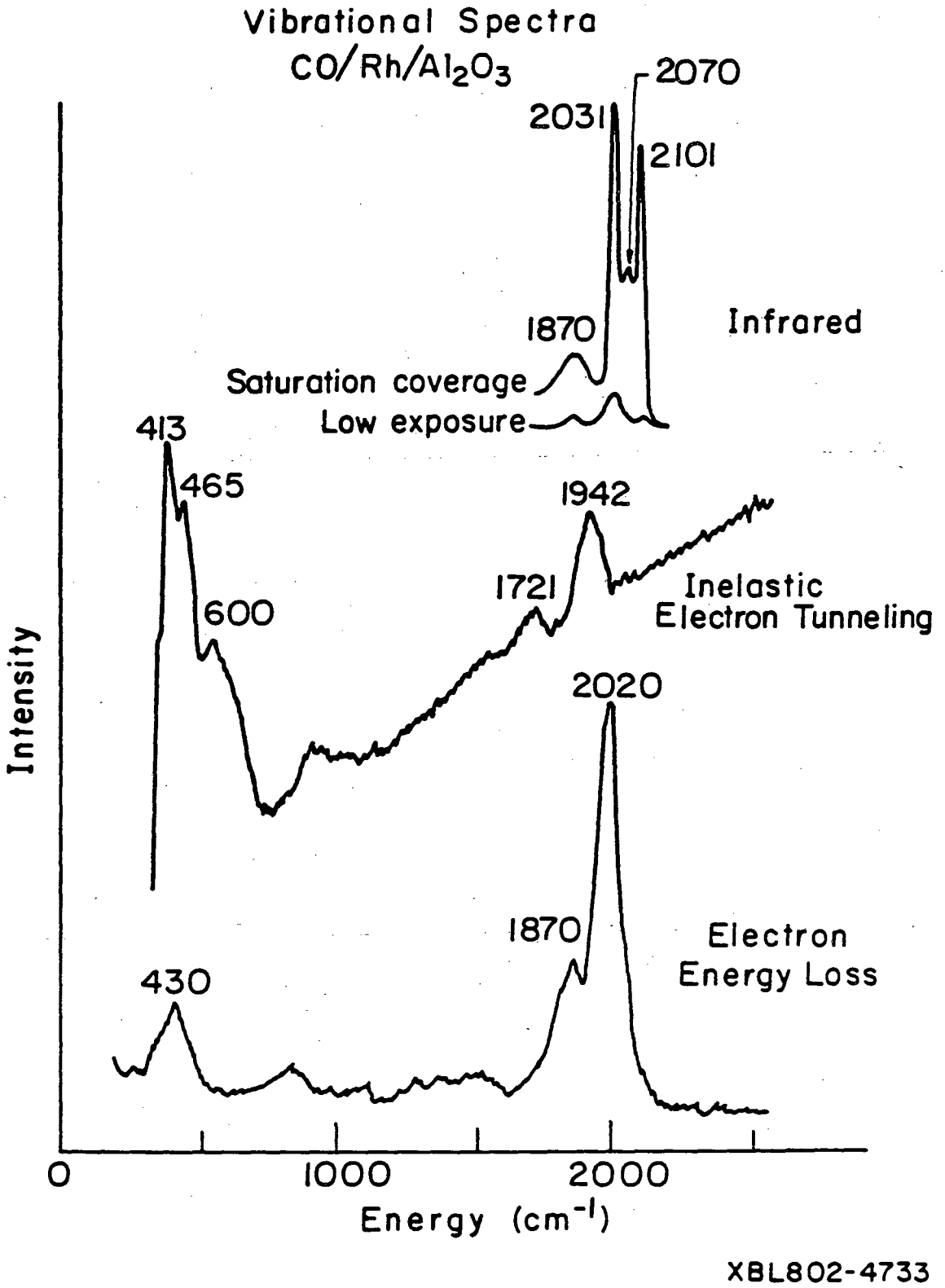
Vibrational Spectra
CO/Rh/Al2O3
2070
2031
2101
1870
Infrared
Saturation coverage
Low exposure
413
465
600
1942
1721
Inelastic
Electron Tunneling
2020
1870
430
Electron
Energy Loss
Intensity
0
1000
2000
Energy (cm-1)
XBL802-4733

Fig. 20

This report was done with support from the Department of Energy. Any conclusions or opinions expressed in this report represent solely those of the author(s) and not necessarily those of The Regents of the University of California, the Lawrence Berkeley Laboratory or the Department of Energy.

Reference to a company or product name does not imply approval or recommendation of the product by the University of California or the U.S. Department of Energy to the exclusion of others that may be suitable.

TECHNICAL INFORMATION DEPARTMENT
LAWRENCE BERKELEY LABORATORY
UNIVERSITY OF CALIFORNIA
BERKELEY, CALIFORNIA 94720